NACA

RESEARCH MEMORANDUM

FLIGHT INVESTIGATION FROM MACH NUMBER 0.8 TO MACH NUMBER 2.0 TO DETERMINE SOME EFFECTS OF WING-TO-TAIL DISTANCE ON THE LONGITUDINAL STABILITY AND CONTROL CHARACTERISTICS OF A 60° DELTA-WING - CANARD MISSILE

By Clarence A. Brown, Jr., and Reginald R. Lundstrom

Langley Aeronautical Laboratory
Langley Field, Va.

NATIONAL ADVISORY COMMITTEE
FOR AERONAUTICS

WASHINGTON

June 20, 1952

Classification cancelled (or changed to UNCLASSIFIED)

By Authority of NASA Tech Pub Announcement #43
(OFFICER DIRECTING CHANGE)

By 2 Apr 57
NAME AND

GRADE OF OFFICER MAKING CHANGE)

3 Apr 57
DATE

NATIONAL ADVISORY COMMITTEE FOR AERONAUTICS

RESEARCH MEMORANDUM

FLIGHT INVESTIGATION FROM MACH NUMBER 0.8 TO MACH NUMBER 2.0 TO DETERMINE SOME EFFECTS OF WING-TO-TAIL DISTANCE ON THE LONGITUDINAL STABILITY AND CONTROL CHARACTERISTICS OF A 60° DELTA-WING - CANARD MISSILE

By Clarence A. Brown, Jr., and Reginald R. Lundstrom

SUMMARY

A flight investigation using rocket-powered models has been made to determine some of the effects of wing-to-tail distance on the stability and control characteristics of a canard-missile configuration having 60° delta wings and control surfaces. Two fuselage lengths, one with the distance between wing and tail 70 percent greater than the other, are compared over a Mach number range from 0.8 to 2.0. Canard hinge moment and model drag data are also presented. Some data are presented on the effect of mounting the canard surfaces on a conical nose.

The results indicate that additional fuselage length increases the lift-curve slope slightly and has very little effect on the minimum drag. The drag at lift is increased slightly. At transonic speeds the movement of the aerodynamic center with Mach number was slightly greater for the longer fuselage. Greater damping was obtained for the long-fuselage model than for the short-fuselage model and for the long-fuselage model the damping increased with increase in trim angle of attack over the range investigated. Hinge moments were very small at supersonic speeds for a 60° delta control surface hinged at 64-percent root chord and comparison with data obtained from a similar control surface having 77 percent greater canard area shows fair agreement.

INTRODUCTION

The Langley Pilotless Aircraft Research Division has conducted a series of free-flight tests to determine the stability and control

characteristics of canard-missile configurations. Reference 1 gives the results of one of these tests and presents the method by which these data were obtained. Reference 2 shows some effects of varying the control-surface area and of interdigitating canards and wings. In order to accommodate additional equipment, it is sometimes necessary to increase the length of a missile after the design is complete and it is usually necessary to insert this additional section between the wing and tail. The present paper presents results of an investigation using the pulsed-control technique to determine some of the effects of this additional body length between wing and tail on the longitudinal stability and control effectiveness derivatives of a canard missile through a Mach number range of approximately 0.80 to 2.0. Canard hinge moment and model drag data are included. Incomplete data are also presented to show some effects of placing the canard surfaces forward on a sharp conical-nose section.

The models used for these tests had 60° delta wings in a cruciform arrangement and 60° delta canard surfaces in the plane of the horizontal wings similar to that in reference 2. For the present investigation, the distance from canard trailing edge to wing trailing edge was increased approximately 70 percent over that of reference 2.

SYMBOLS

$\bar{c}$	wing mean aerodynamic chord of total wing area, feet
S_w	total wing area in one plane including body intercept, square feet
$S_{w_{ex}}$	exposed wing area in one plane, square feet
$\bar{c}_e$	canard-control-surface mean aerodynamic chord of exposed area, feet
S_e	canard-control-surface exposed area, square feet
t	time, seconds
W	weight, pounds
I_y	moment of inertia about Y-axis (pitch axis), slug-feet^2
ρ	mass density of air, slugs per cubic foot
μ	coefficient of viscosity, slugs per foot-second

V	velocity of model, feet per second
V_c	speed of sound in air, feet per second
M	Mach number (V/V_c)
R	Reynolds number $\left(\frac{\rho V \bar{c}}{\mu}\right)$
q	dynamic pressure, pounds per square foot $\left(\frac{1}{2}\rho V^2\right)$ or pitching velocity, radians per second
g	acceleration due to gravity, 32.2 feet per second^2
α	angle of attack, degrees
ϵ	downwash angle, degrees

$\dot{\alpha} = \frac{d\alpha}{dt}$, radians per second

δ_e	canard control deflection, degrees
a_n/g	normal accelerometer reading, g units
a_l/g	longitudinal accelerometer reading, deceleration positive, g units
H	hinge moment, foot-pounds
a.c.	aerodynamic center
C_L	lift coefficient $\left(a_n/g \cos \alpha - a_l/g \sin \alpha\right)W/qS_w$
C_D	drag coefficient $\left(a_l/g \cos \alpha + a_n/g \sin \alpha\right)W/qS_w$
C_m	pitching-moment coefficient about model center of gravity $\left(\frac{\text{Pitching moment}}{qS_w\bar{c}}\right)$
C_h	hinge-moment coefficient $\left(H/qS_e\bar{c}_e\right)$

$\Delta\alpha_{trim}$, $\Delta\delta_e$, $\Delta C_{L_{trim}}$, $\Delta C_{h_{trim}}$ — total change in variable between $\delta_e = -6^\circ$ and $\delta_e = 4^\circ$

α_{trim} — trim angle of attack, degrees

$C_{L_\alpha} = \frac{\partial C_L}{\partial \alpha}$, per degree

$C_{m_\alpha} = \frac{\partial C_m}{\partial \alpha}$, per degree

$\left(C_{m_\alpha}\right)_\psi$ — slope of yawing-moment curve, based on S_w and $\bar{c}$, as determined from transverse accelerometer, per degree

$C_{m_q} + C_{m_{\dot{\alpha}}} = \frac{\partial C_m}{\partial \frac{q\bar{c}}{2V}} + \frac{\partial C_m}{\partial \frac{\dot{\alpha}\bar{c}}{2V}}$, per radian

$C_{L_{\delta_e}} = \frac{\partial C_L}{\partial \delta_e}$, per degree

$C_{m_{\delta_e}} = \frac{\partial C_m}{\partial \delta_e}$, per degree

$C_{h_\alpha} = \frac{\partial C_h}{\partial \alpha}$, per degree

$C_{h_{\delta_e}} = \frac{\partial C_h}{\partial \delta_e}$, per degree

$C_{D_{min}}$ — minimum drag coefficient

P — period, seconds

b — exponential damping constant in e^{-bt}, per second

APPARATUS AND METHODS

Model

Sketches of the rocket-powered models used in these tests and details of canards are shown in figures 1 and 2. Photographs of the models are shown in figure 3. The physical characteristics of the models are given in the following table:

	Model A ogival nose	Model B conical nose
Wing:		
S_w, sq ft	2.835	2.835
$\bar{c}$, ft	1.463	1.463
Thickness/chord at body juncture	0.030	0.030
$S_{w_{ex}}$, sq ft	1.70	1.70
Wing span, ft	2.58	2.58
Canard control surfaces:		
S_e, sq ft	0.1083	0.1083
$\bar{c}_e$, ft	0.289	0.265
Thickness/chord at body juncture	0.031	0.028
Hinge line percent root chord	64.0	63.6
Control-surface span, ft	1.08	0.81
General:		
Weight, pounds	123.0	124.3
I_y, slug-ft^2	52.16	41.22
Body diameter, in	7.0	7.0
Fineness ratio	22.04	20.89
$S_e/S_{w_{ex}}$	0.064	0.064
Tail length, trailing edge of control surface to trailing edge of wing, ft	8.06	8.05
Span of control surface/span of wing	0.42	0.31

The fuselage of model A was cylindrical with an ogival nose and tail section. The 60° delta wings and canard control surfaces were mounted on the cylindrical section of the body. The solid-duralumin delta wings were fixed on the all-metal airframe in cruciform arrangement. The solid-steel control surfaces were located only in the plane of the horizontal wings. The only difference between model A and

model 1 of reference 2 is the addition of a 40-inch section of fuselage between the canard surface and the wing, which increased the distance between wing and tail by about 70 percent.

The fuselage of model B was cylindrical with a conical nose and an ogival tail section. The canard control surfaces were located on the conical nose section in the plane of the horizontal wings and pivoted about a hinge line perpendicular to the body center line. The control-surface root chord of model B was taken as a line drawn from the most forward point on the canard surface perpendicular to the trailing edge (fig. 2). The control-surface exposed area and the distance from the control-surface hinge lines to the wings are the same for models A and B. The wings of models A and B were identical.

The canard control surfaces of both models were pulsed in a square-wave motion by deflecting them abruptly to 4° and holding them in this position for a predetermined time interval, then deflecting them again abruptly to -6° and holding them again at this deflection for the same time; this sequence was repeated throughout the flight of the model. The control surfaces were actuated by a hydraulic servomotor, the fluid being supplied by an accumulator and programmed by a motor-driven valve. The time interval for a fixed control deflection was 0.7 second during supersonic flight and was increased to 1.2 seconds during transonic flight in order to allow for the slower response of the model. This was accomplished by using a pressure switch connected to the total-pressure tube to decrease the voltage to the electric motor which drives the hydraulic programming valve.

Each model was boosted to supersonic velocities by two solid propellant rocket motors which together delivered approximately 13,000 pounds of thrust for 3.0 seconds. Both models were launched at an angle of approximately 60° to the horizontal.

Instrumentation

The models were equipped with NACA nine-channel telemeters which transmitted a continuous record of normal (two ranges), longitudinal, and transverse accelerations, angle of attack, control deflection, control hinge moment, total and static pressures.

Velocity was obtained from the CW Doppler radar unit and from the total-pressure pickup. In general, the agreement between the two methods was within ± 0.5 percent. The trajectory of the model was determined by means of a radar tracking unit and a radiosonde was used to obtain atmospheric data throughout the altitude range traversed by the model.

Fuselage Rigidity

In order to minimize the effects of fuselage bending so that comparison of results could be made with reference 2 on a basis of aerodynamic effects only, the models were made as rigid as possible. Before launching, the bending stiffness was determined experimentally at various stations along the fuselage. The experimental values of stiffness and estimated aerodynamic and inertia loads were used to calculate the slope of the deflection curve at the angle-of-attack indicator, the canard surfaces, and the horizontal wing. The differences between these three slopes were less than one-tenth of a degree under a normal acceleration of 20g.

Method of Analysis

Each time the control-surface deflection changed, the model responded by oscillating about a new trim position. The angle-of-attack indicator reading was corrected to give the angle of attack at the center of gravity except in the case of canard hinge moment where correction was made to the hinge line. The method used in making these corrections is given in reference 3. Lift and drag coefficients were determined from the normal and longitudinal accelerometer readings as follows:

$$C_L = \left(a_n/g \cos \alpha - a_l/g \sin \alpha\right) W/qS_w$$

and

$$C_D = \left(a_l/g \cos \alpha + a_n/g \sin \alpha\right) W/qS_w$$

The damping derivative $C_{m_q} + C_{m_{\dot{\alpha}}}$ was obtained from the rate of decay of the pitching motion with proper allowances being made for the contribution of vertical translation to the damping. The pitching-moment derivative, C_{m_α} and the yawing-moment derivative, $\left(C_{m_\alpha}\right)_\psi$ were obtained from the period of the normal and transverse accelerations, respectively. The symbol $\left(C_{m_\alpha}\right)_\psi$ is representative of the pitching-moment derivative C_{m_α} of the configuration with canard surfaces removed. Control effectiveness derivatives $C_{L_{\delta_e}}$ and $C_{m_{\delta_e}}$ were obtained from the relationships:

$$\Delta C_{L_{trim}} = C_{L_{\delta_e}}(\Delta\delta_e) + C_{L_\alpha}(\Delta\alpha_{trim})$$

$$C_{m_\alpha}(\Delta\alpha_{trim}) = C_{m_{\delta_e}}(\Delta\delta_e)$$

Only an average $C_{L_{\delta_e}}$ and $C_{m_{\delta_e}}$ for the range $\delta_e = 4^\circ$ to $\delta_e = -6^\circ$ could be obtained because it was necessary to account for the out-of-trim lift and pitching moment. By making plots of C_h against α for constant δ_e, it was possible to obtain values of the slope C_{h_α}. Hinge-moment coefficient due to δ_e, $C_{h_{\delta_e}}$ was obtained from the relationship:

$$\Delta C_{h_{trim}} = C_{h_{\delta_e}}(\Delta\delta_e) + C_{h_\alpha}(\Delta\alpha_{trim})$$

A more extensive derivation of this method of analysis is given in the appendix of reference 1.

Accuracy

The accuracy of the stability and control derivatives, drag, and hinge-moment coefficients when possible cumulative errors in radar and telemeter data are considered is believed to be within the limits listed below for two Mach numbers.

M	Percent of given value						
	C_{L_α}	C_{m_α}	$C_{L_{\delta_e}}$	$C_{m_{\delta_e}}$	$C_{m_q} + C_{m_{\dot{\alpha}}}$	C_h	C_D
0.80	5	6	50	8	25	5	8
1.80	3	4	45	6	15	5	4

The accuracy of $C_{L_{\delta_e}}$ is poor because for this particular configuration $C_{L_{\delta_e}}$ is very small compared to C_{L_α}.

RESULTS AND DISCUSSION

Complete data were received on model A for a Mach number range of 0.8 to 2.0. Although data were received below 0.8 Mach number, because of the low velocity and high altitude, the period was so long and the normal accelerations so low that reduction of the data was impractical. During the free fall from the peak of the trajectory, the model accelerated to a Mach number of approximately 0.86 just before impact. The dynamic pressure before impact was 1045 pounds per square foot whereas at 18,000 feet, the point on upward trajectory where model was at a Mach number of 0.86, the dynamic pressure was 512 pounds per square foot. The data obtained just before impact are included for comparison. Model B provided very little data because a failure in the pulse system caused the control surface to pulse only once. These data are included on the same figures as model A.

The Reynolds number of these tests ranged from approximately 4×10^6 to 21×10^6 based on wing mean aerodynamic chord. Variation of Reynolds number with Mach number for these tests is shown in figure 4.

Lift

Typical plots of C_L against α are shown in figure 5 at three Mach numbers for model A and one Mach number for model B. A plot of lift-curve slope against Mach number for model A and available data from model B are presented in figure 6. Included in this figure for comparison is the lift-curve slope of model 1 in reference 2. Comparison of the lift-curve slopes for model A at a δ_e of 4° and δ_e of -6° shows them to be practically the same. The lift-curve slopes obtained just before impact, Mach number approximately 0.86, also agree favorably with those obtained at about 18,000 feet at the same Mach number. It is evident that at Mach numbers of about 1.9 the lift-curve slope of the model with canard surfaces on the conical nose section, model B, is greater than the lift-curve slope of the model with the canard surfaces on the cylindrical portion of the body (model A). This difference may be due to the fact that the canard span of model B is shorter and thus causes less of the main wing surface to be in the downwash field. The data indicate that the model with the long fuselage, model A, had a greater lift-curve slope by about 7 percent at supersonic speeds than the similar model with the shorter fuselage (model 1, ref. 2) although below a Mach number of 0.85 it is the same. This increase in C_{L_α} for the model with the longer body can be attributed to decreased downwash and increased body lift or both.

Pitching Moments

The static stability of the model as obtained from the plot of the period against Mach number in figure 7 is presented in figure 8 as C_{m_α} as a function of Mach number and in figures 9 and 10 as aerodynamic-center position as a function of Mach number.

The trend of the static stability with Mach number is similar to those presented in references 1 and 2 for the shorter tail length. At supersonic speed the stability of model A was greater at the numerically greater δ_e and corresponding α trim. This is in agreement with wind-tunnel tests on canard missiles with delta wing and canard surfaces, for example reference 4 which shows the slope of the curve of C_m as a function of α increasing with an increase in α. Figures 8, 9, and 10 show that the data obtained just before impact for the 4° control deflection are in rather poor agreement with that obtained at 18,000 feet altitude. The fact that these low-altitude data are available only in the Mach number range where the center of pressure is changing rapidly may at least partially explain this disagreement.

Each time the control surface was deflected abruptly, it also disturbed the model in a transverse direction. The amplitude of the resulting transverse motion, however, was only about one-tenth the amplitude of the normal motion. The resulting transverse oscillation had a different period (fig. 7) from the normal oscillation and close inspection failed to disclose any evidence of coupling between the two modes. The stability derivative $\left(C_{m_\alpha}\right)_\psi$ was calculated from the period of the transverse oscillation by assuming only the rotational degree of freedom. Calculations of C_{m_α} showed that accounting for the translational degree of freedom changed the results by less than 2 percent. Much wind-tunnel data, for example reference 5, have shown that the presence of canards in one plane have negligible effect on the static stability in the other plane. Thus, the plot of $\left(C_{m_\alpha}\right)_\psi$ is included in figure 8 to show the difference in stability with and without canard surfaces. It may be seen that the canard surfaces greatly reduce the stability at transonic and low supersonic speeds, whereas at about $M = 1.85$ the presence of the canards apparently has somewhat less effect on the stability.

Figure 8 shows that model B was more stable than model A. Because of atmospheric disturbances, some points for $\left(C_{m_\alpha}\right)_\psi$ were obtained for model B at about $M = 1.5$ which are higher than those obtained for model A at the same Mach number. This difference indicates that at least part of the increased stability of model B is caused by the fuselage nose shape itself.

Figure 9 compares the aerodynamic-center position as a function Mach number with the aerodynamic-center position of model 1 of reference 2. At supersonic speeds the direction of travel of the aerodynamic center with increasing Mach number is about the same for both model A and model 1 of reference 2, but at transonic speeds a somewhat greater movement is indicated for the model with the long fuselage. Figure 10 shows the actual position of the aerodynamic center on the body for models A and B as a function of Mach number. As may be seen, at Mach number of 1.87 to 1.95, the aerodynamic center of the model with the conical nose was more rearward than for the model with the ogival nose.

Damping in Pitch

The damping in pitch for model A was calculated from the rate of decay of the pitching motion following each control movement. The logarithmic decrement b is presented as a function of Mach number in figure 11. The coefficient $C_{m_q} + C_{m_{\dot{\alpha}}}$ as obtained from these values of b is presented as a function of Mach number in figure 12. Included also are some data from model B. It may be noted that a large difference in damping exists between $\delta_e = -6^\circ$ and $\delta_e = 4^\circ$. This difference suggests that probably the center of pressure of the lifts on the wing due to model pitching may be farther forward at $\delta_e = 4^\circ$ than at $\delta_e = -6^\circ$ just as the center of pressure of the lift on the wing due to angle of attack must have been farther forward at $\delta_e = 4^\circ$ than at $\delta_e = -6^\circ$ in order to give the center-of-pressure positions shown in figure 9. Figure 12 also shows that there is a marked reduction in damping at transonic speeds and indicates an increase in $C_{m_q} + C_{m_{\dot{\alpha}}}$ at subsonic speeds over the supersonic values. Also included in the plot are the points from model A obtained just before impact which are in very good agreement with the values of $C_{m_q} + C_{m_{\dot{\alpha}}}$ obtained at 18,000 feet altitude. Because the center of gravity was 9.7 inches farther forward of the main wing in the case of the long model, little basis for comparison exists between the damping of the short- and long-fuselage models. As would be expected, however, the damping coefficient $C_{m_q} + C_{m_{\dot{\alpha}}}$ was much greater for the model with the long fuselage as shown in figure 12.

Trim Angle of Attack and Control Effectiveness

Plots of trim angle of attack for both control deflections are presented in figure 13. These values are actual measured values and include any out of trim due to misalinements.

Some idea of the effectiveness of the control surface in producing lift and pitching moment may be obtained from the plots of $C_{L_{\delta_e}}$ and $C_{m_{\delta_e}}$ against Mach number in figures 14 and 15, respectively. It should be pointed out that only the average $C_{L_{\delta_e}}$ and $C_{m_{\delta_e}}$ over the 10° range of $\delta_e = 4^\circ$ to $\delta_e = -6^\circ$ could be determined and no variation of $C_{L_{\delta_e}}$ and $C_{m_{\delta_e}}$ with control deflection could be obtained.

The fact that $C_{L_{\delta_e}}$ is negative means that the loss of lift on the wing due to $\partial\epsilon/\partial\delta_e$ exceeds the lift of the control surface itself. Comparison of $C_{L_{\delta_e}}$ for model A with that obtained from model 1 of reference 2, as presented in figure 14, shows good agreement at supersonic speeds but shows $C_{L_{\delta_e}}$ of the long-fuselage model to have a greater negative value at transonic speeds.

As may be seen in figure 15, the variation with Mach number of $C_{m_{\delta_e}}$ is practically the same as that of C_{m_α}. Because of this similarity, a smooth curve of control response is obtained throughout the entire test range.

Hinge Moments

Variation of hinge-moment coefficient with angle of attack C_{h_α} and variation of hinge-moment coefficient with control deflection $C_{h_{\delta_e}}$ are presented in figure 16 as a function of Mach number. Comparison of $C_{h_{\delta_e}}$ and C_{h_α} with the data from a similar model with 77 percent greater exposed area of the canard surface (ref. 1) shows fair agreement. The high values of C_{h_α} at Mach numbers of 0.955 and 0.970, shown in figure 16, are undoubtedly caused by a large forward movement of the control-surface center of pressure. Plots of C_h against α in this Mach number range, however, still showed good linearity. Both control deflections $\delta_e = -6^\circ$ and $\delta_e = 4^\circ$ for model A yielded the same C_{h_α} within the accuracy of the method. The single value of C_{h_α}, $M = 1.92$, obtained for model B was the same as for model A.

Drag

The variation of drag coefficient with lift coefficient is shown in figure 17 for Mach numbers ranging from 0.8 to 2.0. Minimum drag coefficients obtained from figure 17 are shown in figure 18. A comparison of minimum drag coefficients for model A with model 1 from reference 2 presented in figure 18 shows that the extra length fuselage did not increase the drag coefficient within the accuracy of the tests. Because of the failure of the pulsing system of model B a comparison between the drag coefficients of models A and B through the Mach number range was possible only at the trim lift coefficient of model B. This comparison, as shown in figure 19, indicates the drag coefficient of the two models to be practically the same at supersonic speeds but the drag coefficient of the cone-cylinder configuration is slightly greater at transonic speeds. All models compared had angle-of-attack indicators on the model nose (fig. 1) and these drag data include any effects of the indicator on the model drag coefficient.

Variation of Drag with Lift

The drag parameter $\frac{dC_D}{dC_L^2}$ as a function of Mach number is presented in figure 20 for model A and for model 1 from reference 2. The data for both models are in the range $C_L = 0$ to $C_L = 0.25$. The agreement is generally good with the long-fuselage model having slightly higher $\frac{dC_D}{dC_L^2}$ throughout the Mach number range. Plots of $\frac{1}{57.3} C_{L_\alpha}$ for both models are included in figure 20 for comparison.

For an example of the drag penalty of the extra length of fuselage, consider both models flying at $M = 1.8$ and $C_L = 0.25$. Reference to figures 18 and 20 shows that the short-fuselage model would have a total C_D of 0.0745 $\left(C_{D_{min}} = 0.0435 \text{ plus } C_D \text{ due to lift} = 0.031\right)$ whereas the long-fuselage model would have a total C_D of 0.0773 $\left(C_{D_{min}} = 0.0438 \text{ plus } C_D \text{ due to lift of } 0.0335\right)$ which is about 3.8 percent higher drag than the short model.

Comparison of Actual and Calculated Motions

The stability and control derivatives of model A as determined from these tests were inserted in the equations of motion for two degrees of

freedom (rotation in pitch and vertical translation) and the angle of attack and normal acceleration responses of the model were calculated for the two control-surface positions. A comparison of these calculated responses with the actual measured responses of the model is presented in figures 21 and 22 for the two Mach numbers indicated. As may be seen, the agreement is good.

Frequency Response

The transfer function α/δ of model A as calculated from the equations of motion considering two degrees of freedom longitudinally are

$$\frac{\alpha}{\delta}(D) = \frac{CFD - (CF + AH)}{-AED^2 + (AF + AJ - BE)D + (AG + BF)}$$

where

$$A = \frac{m\dot{V}}{57.3qS_w} \qquad J = \frac{C_{m_{\dot{\alpha}}}\bar{c}}{(57.3)(2)(V)}$$

$$B = C_{L_\alpha} \qquad G = C_{m_\alpha}$$

$$C = C_{L_\delta} \qquad H = C_{m_\delta}$$

$$E = \frac{I_y}{57.3qS_w\bar{c}} \qquad C_{m_q} \text{ assumed to be } = 0.90\left(C_{m_q} + C_{m_{\dot{\alpha}}}\right)$$

$$F = \frac{C_{m_q}\bar{c}}{(57.3)(2)(V)} \qquad D = \frac{d}{dt}$$

The phase and amplitude of the angle-of-attack response α to a control deflection δ is obtained by substituting $i\omega$ for D in the above expression of α/δ. This substitution gives a complex number. The phase angle ϕ can be expressed $\tan^{-1}\frac{\text{Imaginary part}}{\text{Real part}}$ and the amplitude of α/δ is $\sqrt{(\text{Imaginary part})^2 + (\text{Real part})^2}$. These expressions were reduced from the equations of motion adapted from reference 6.

Frequency-response characteristics for model A are presented in figures 23 and 24 for $\delta_e = 4^\circ$ and $\delta_e = -6^\circ$.

CONCLUSIONS

Data obtained from the flight of a canard missile configuration having an ogival nose, 60° delta wings, and canard surfaces, and with a large wing to tail distance, when compared with data from a similar model with a section of fuselage between wing and tail removed, indicate the following:

1. Lift-curve slope for the long model was about 7 percent greater than that for the short model.

2. The damping derivative $C_{m_q} + C_{m_{\dot{\alpha}}}$ was less at supersonic speeds than at subsonic speeds in the case of the long model and less at transonic speeds than either subsonic or supersonic speeds for both models. $C_{m_q} + C_{m_{\dot{\alpha}}}$ was much larger for the longer-fuselage model. For the long-fuselage model $C_{m_q} + C_{m_{\dot{\alpha}}}$ increased with increase in trim angle of attack over the range investigated.

3. The aerodynamic-center position was nearly constant at supersonic speeds for both models. At transonic speeds the movement of the aerodynamic center with Mach number was greater for the long model than for the short model.

4. The effectiveness of control surfaces in producing lift $C_{L_{\delta_e}}$ was very small and negative at transonic and supersonic speeds for both models. The pitching effectiveness of control surfaces $C_{m_{\delta_e}}$ varied smoothly with Mach number in much the same way as for the model with the shorter fuselage.

5. The addition of the extra length of fuselage did not noticeably increase the minimum drag but increased the drag at lift slightly.

Data obtained from the flight of a model with an ogival nose and canards on the cylindrical part of the fuselage when compared with data from a similar model with a conical nose and canards forward on the conical section indicate the following:

1. When compared at Mach number of 1.95 (only place comparison is possible) the lift-curve slope was greater and the aerodynamic center more rearward for the model with the conical nose.

2. At supersonic speeds the drag coefficients for both models were practically the same but at transonic speeds the drag coefficient of the cone-cylinder configuration was slightly greater.

Hinge moments were very small at supersonic speeds for a 60° delta control surface hinged at 64 percent root chord and comparison of the hinge-moment coefficient due to angle of attack C_{h_α} and the hinge-moment coefficient due to control deflection $C_{h_{\delta_e}}$ with data obtained from a similar control surface having 77 percent greater canard area shows fair agreement.

Langley Aeronautical Laboratory
National Advisory Committee for Aeronautics
Langley Field, Va.

REFERENCES

1. Niewald, Roy J., and Moul, Martin T.: The Longitudinal Stability, Control Effectiveness, and Control Hinge-Moment Characteristics Obtained from a Flight Investigation of a Canard Missile Configuration at Transonic and Supersonic Speeds. NACA RM L50I27, 1950.

2. Moul, Martin T., and Wineman, Andrew R.: Longitudinal Stability and Control Characteristics From a Flight Investigation of a Cruciform Canard Missile Configuration Having an Exposed Wing-Canard Area Ratio of 16:1. NACA RM L52D24a, 1952.

3. Mitchell, Jesse L., and Peck, Robert F.: An NACA Vane-Type Angle-of-Attack Indicator for Use at Subsonic and Supersonic Speeds. NACA RM L9F28a, 1949.

4. Fischer, H. S.: Data Report on Supersonic Wind Tunnel Tests of a 0.075-Scale Model of the NIKE 484 Missile. Rep. No. SM-14015, Douglas Aircraft Co., Inc., June 14, 1951.

5. Fleming, R. M.: Supersonic Wind Tunnel Tests at M = 2.25 of the MX-770 1000-Mile Missile. Report No. AL-778, North American Aviation, Inc., Oct. 20, 1948.

6. Greenberg, Harry: Frequency-Response Method for Determination of Dynamic Stability Characteristics of Airplanes With Automatic Controls. NACA Rep. 882, 1947. (Supersedes NACA TN 1229.)

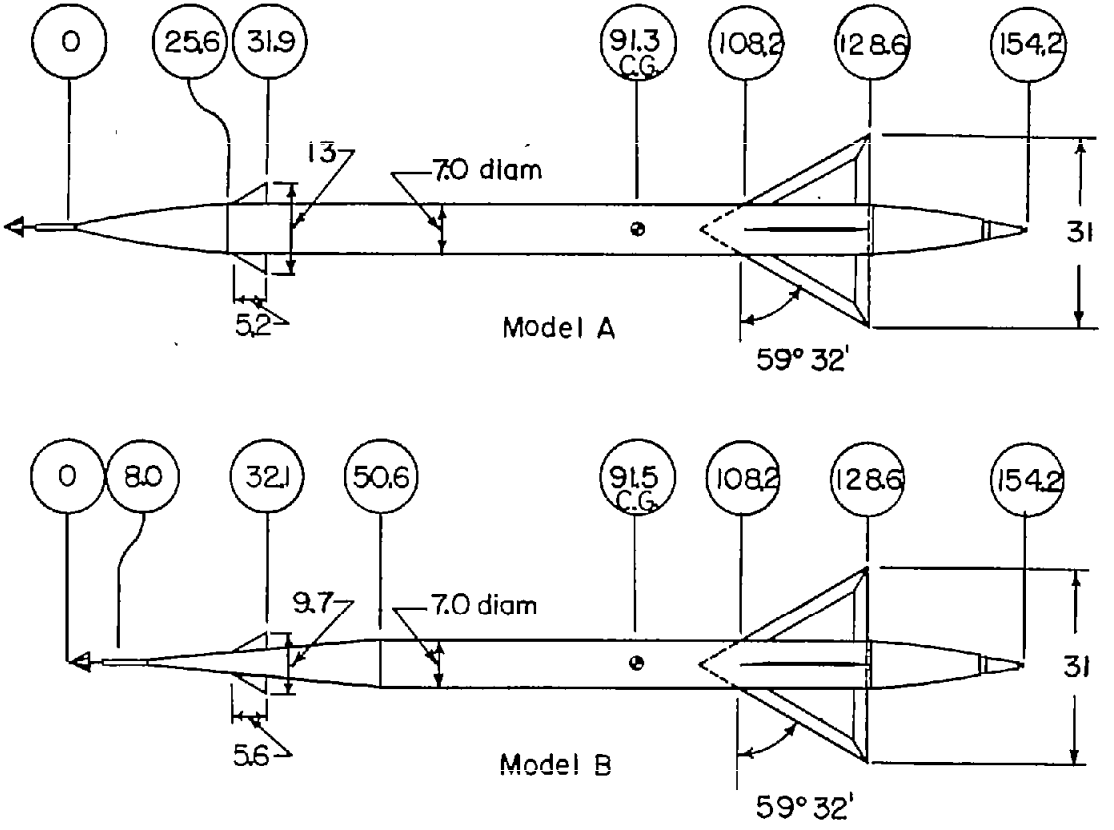

Exposed wing area, sq ft	1.700
Total wing area, sq ft	2.835
Exposed control surface area, sq ft	.108

Figure 1.- Sketch of models tested. All dimensions in inches.

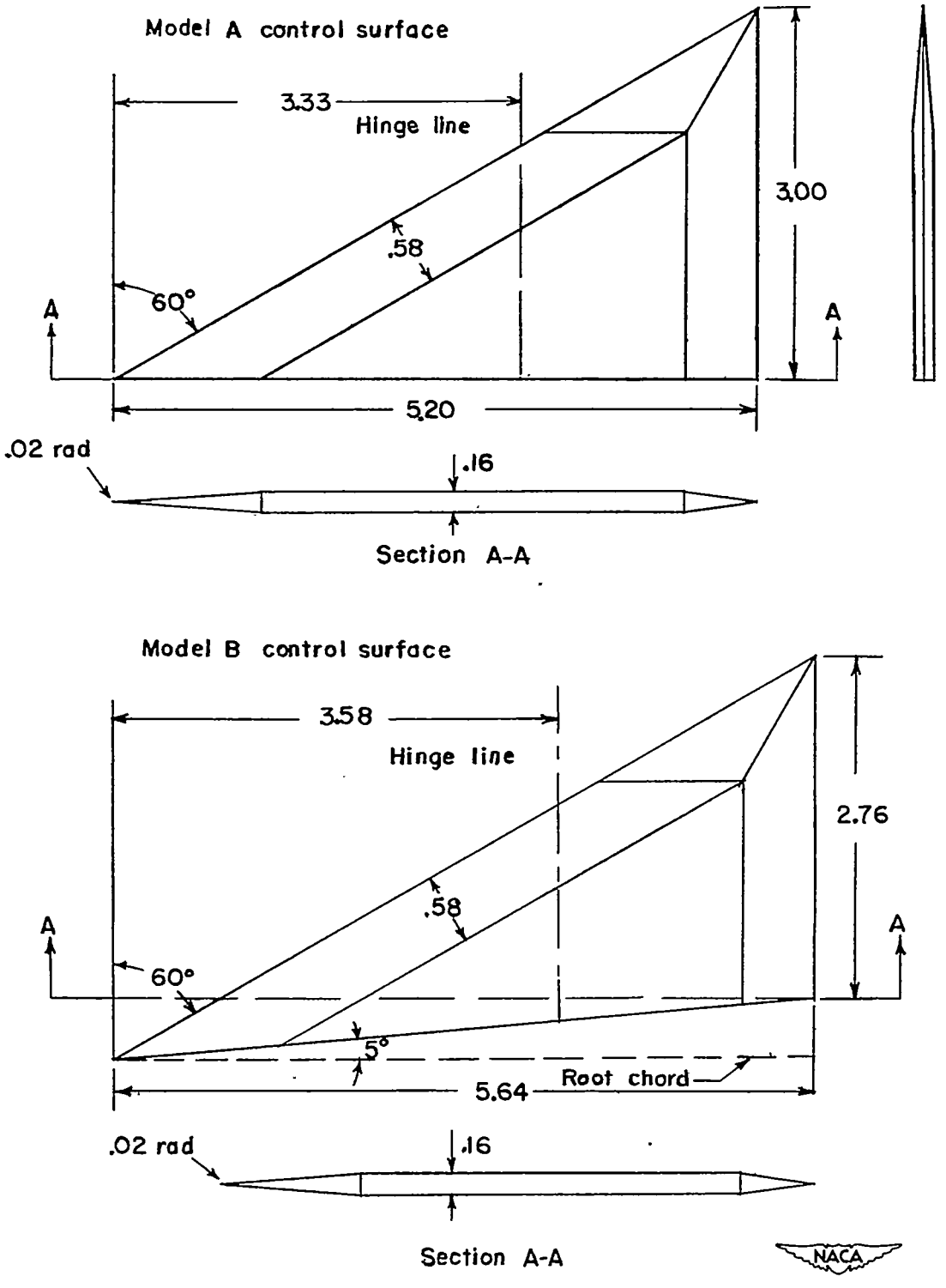

Figure 2.- Sketch of control-surfaces for both models tested. All dimensions in inches.

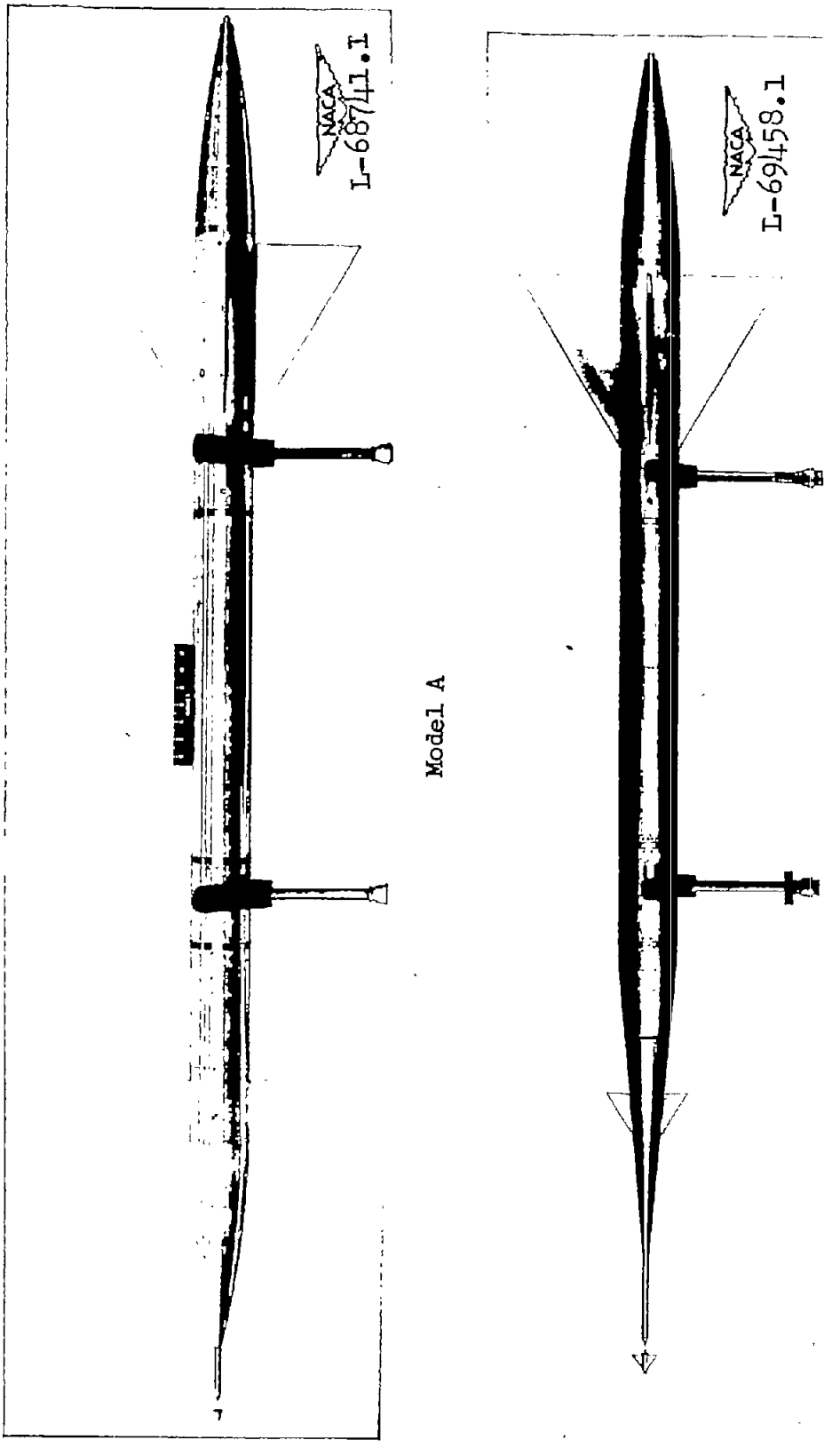

Figure 3.- Photographs of models tested.

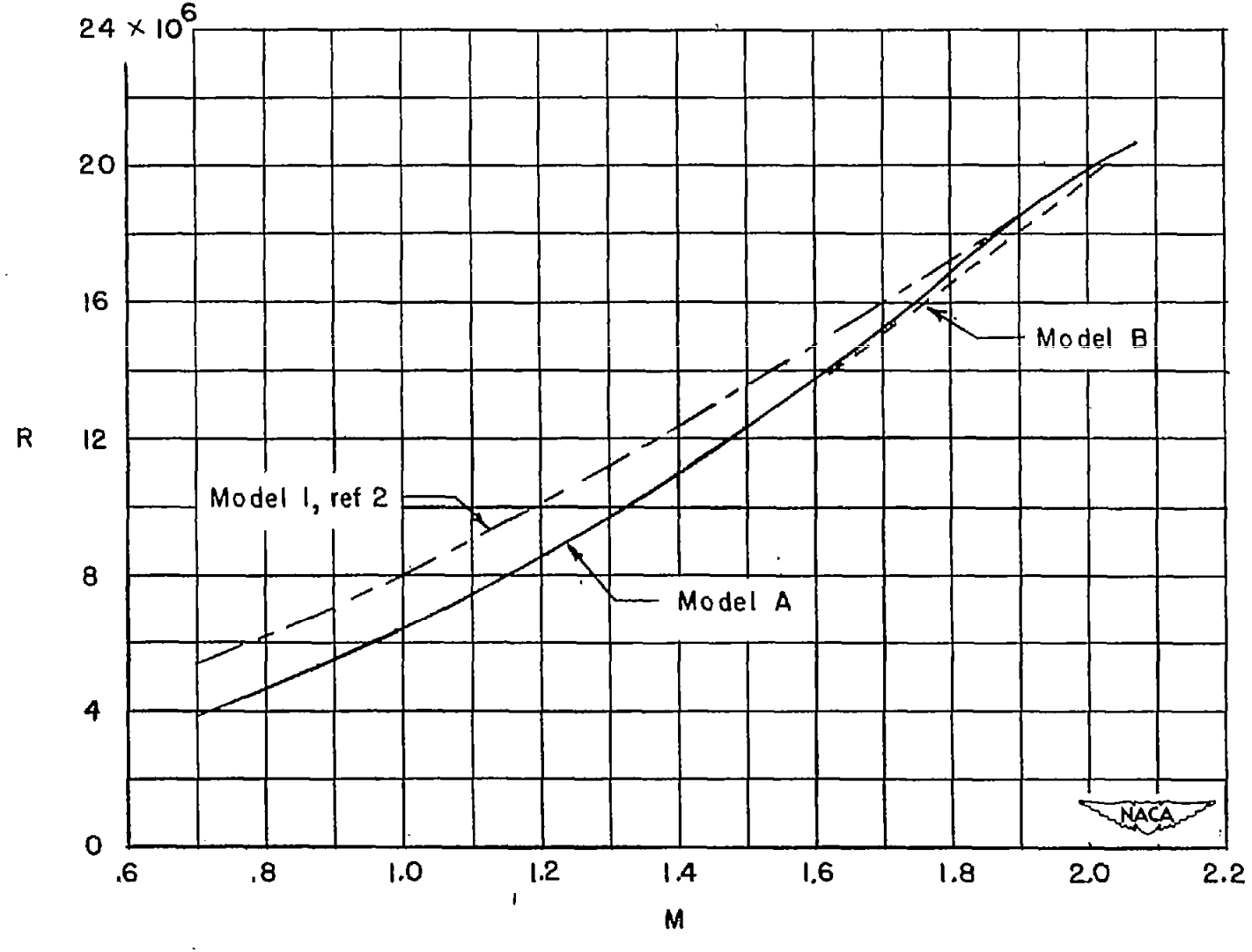

Figure 4.- Reynolds number variation with Mach number.

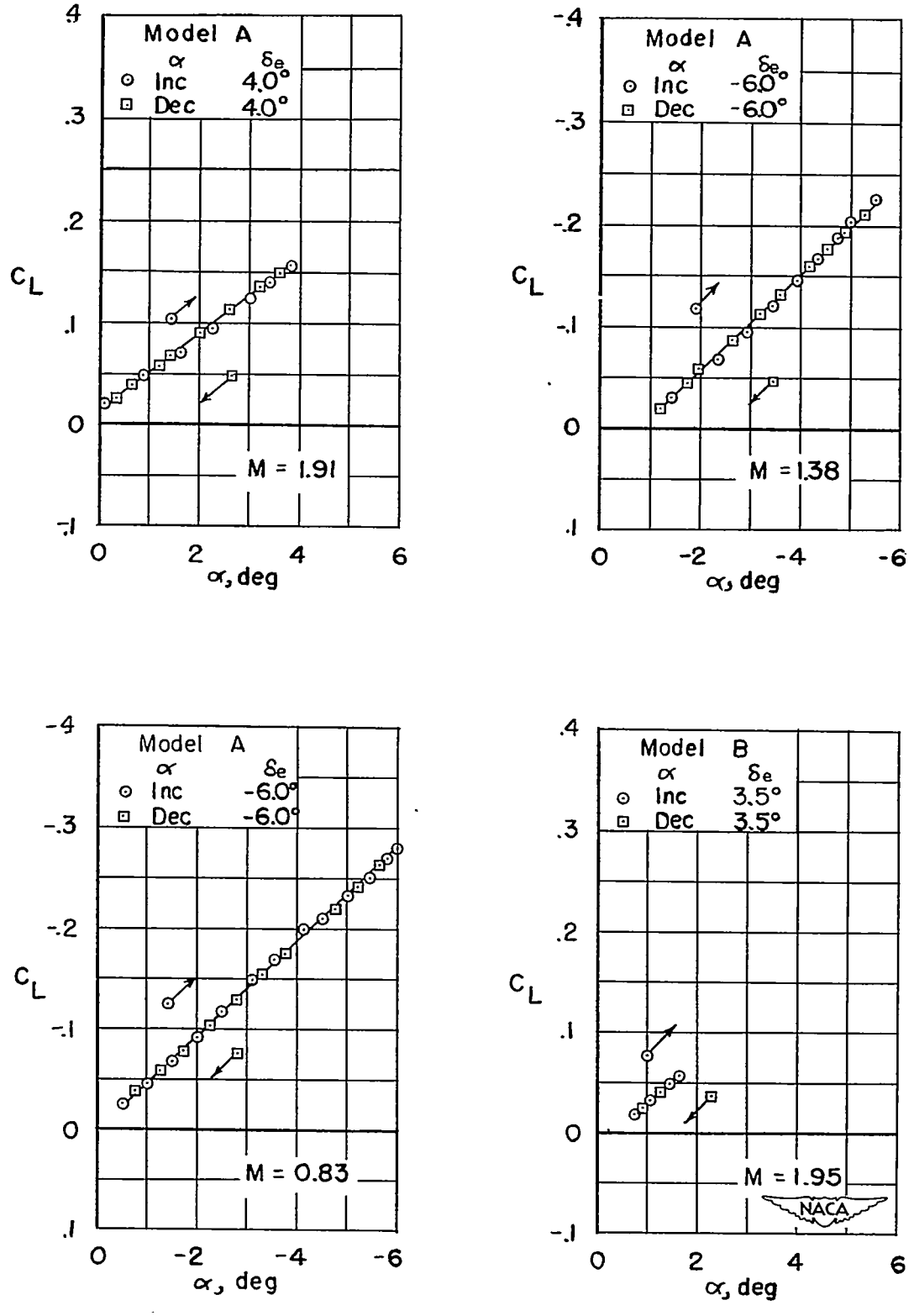

Figure 5.- Variation of lift coefficient with angle of attack.

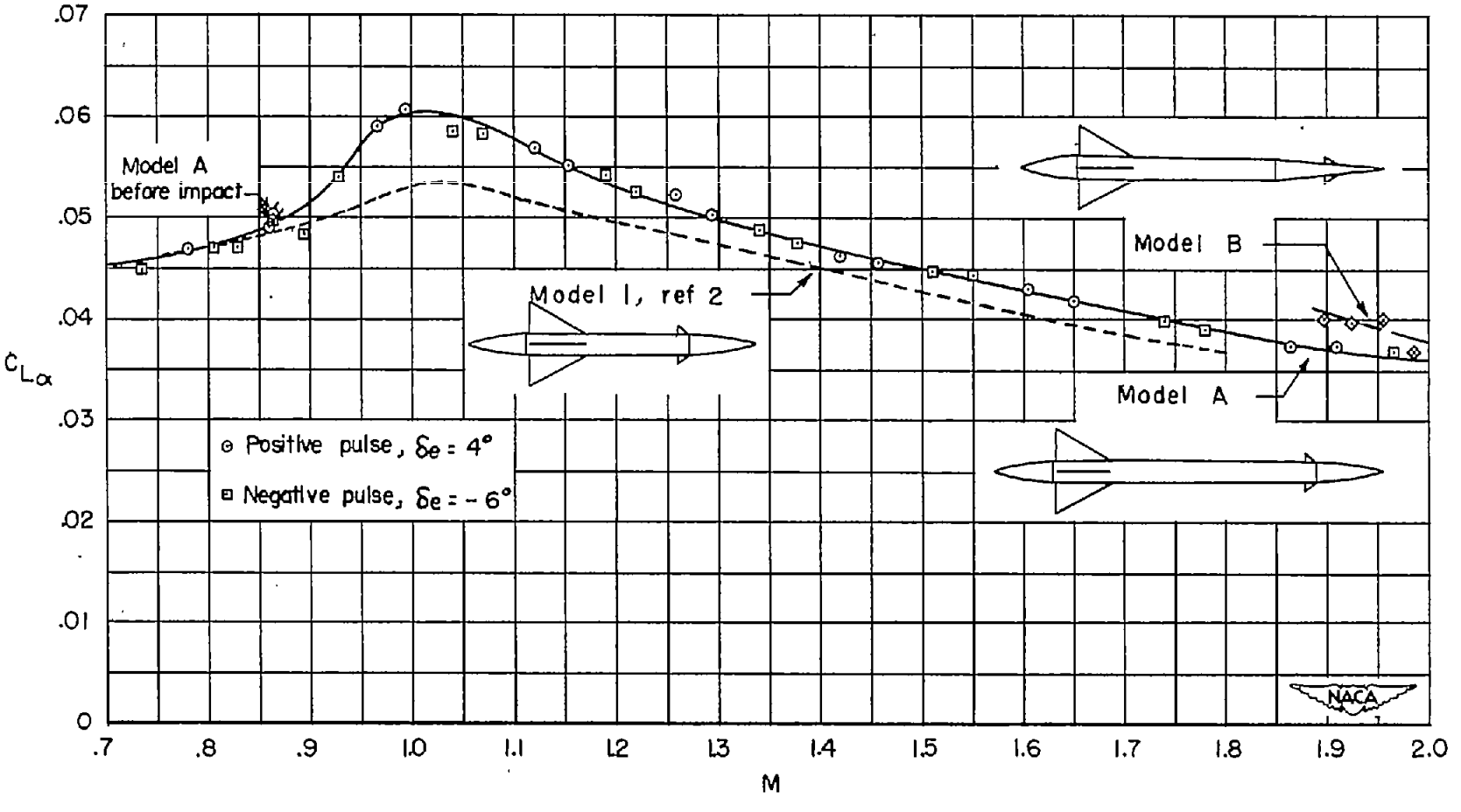

Figure 6.- Variation of lift-curve slope with Mach number.

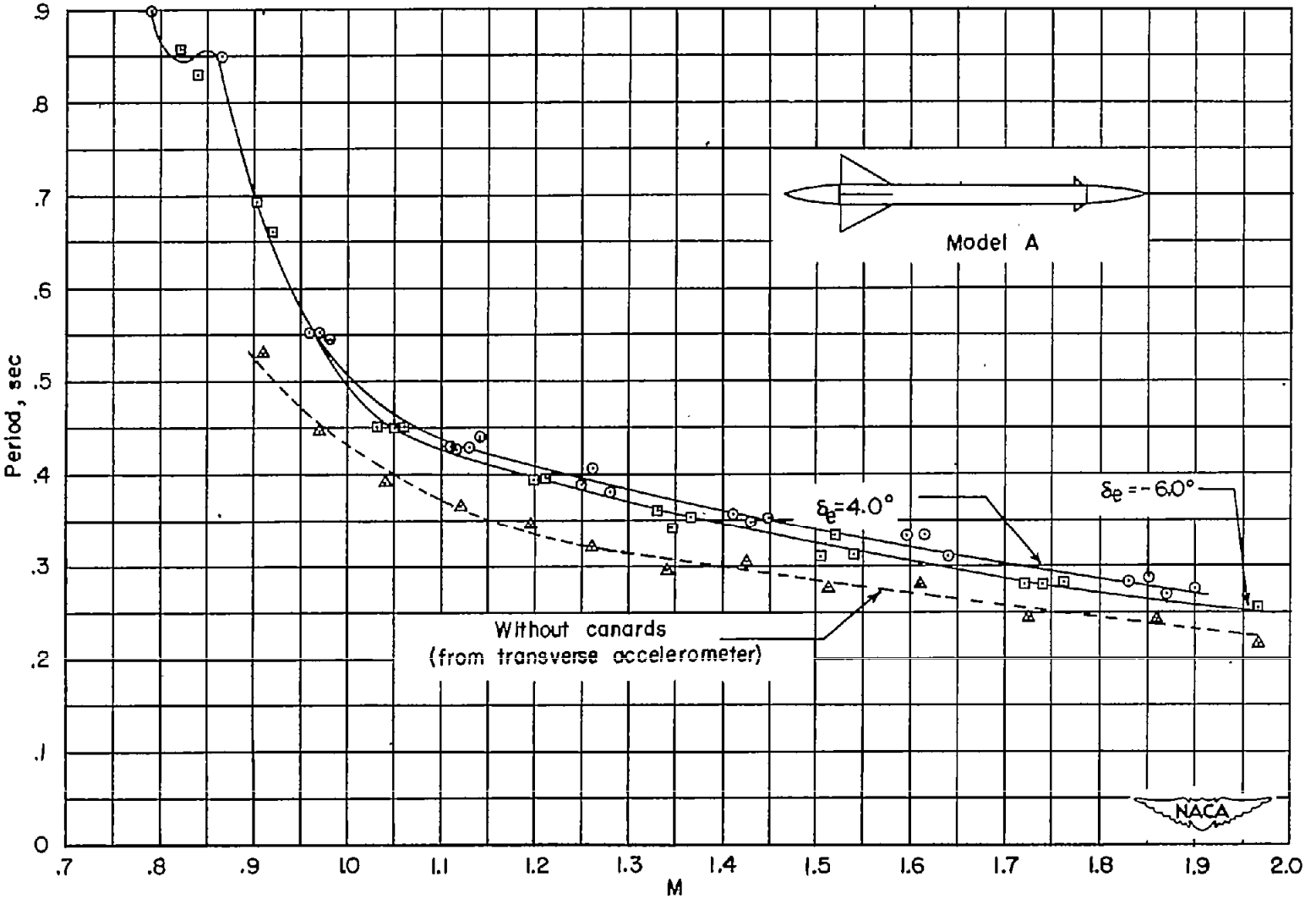

Figure 7.- Variation of period with Mach number for model A.

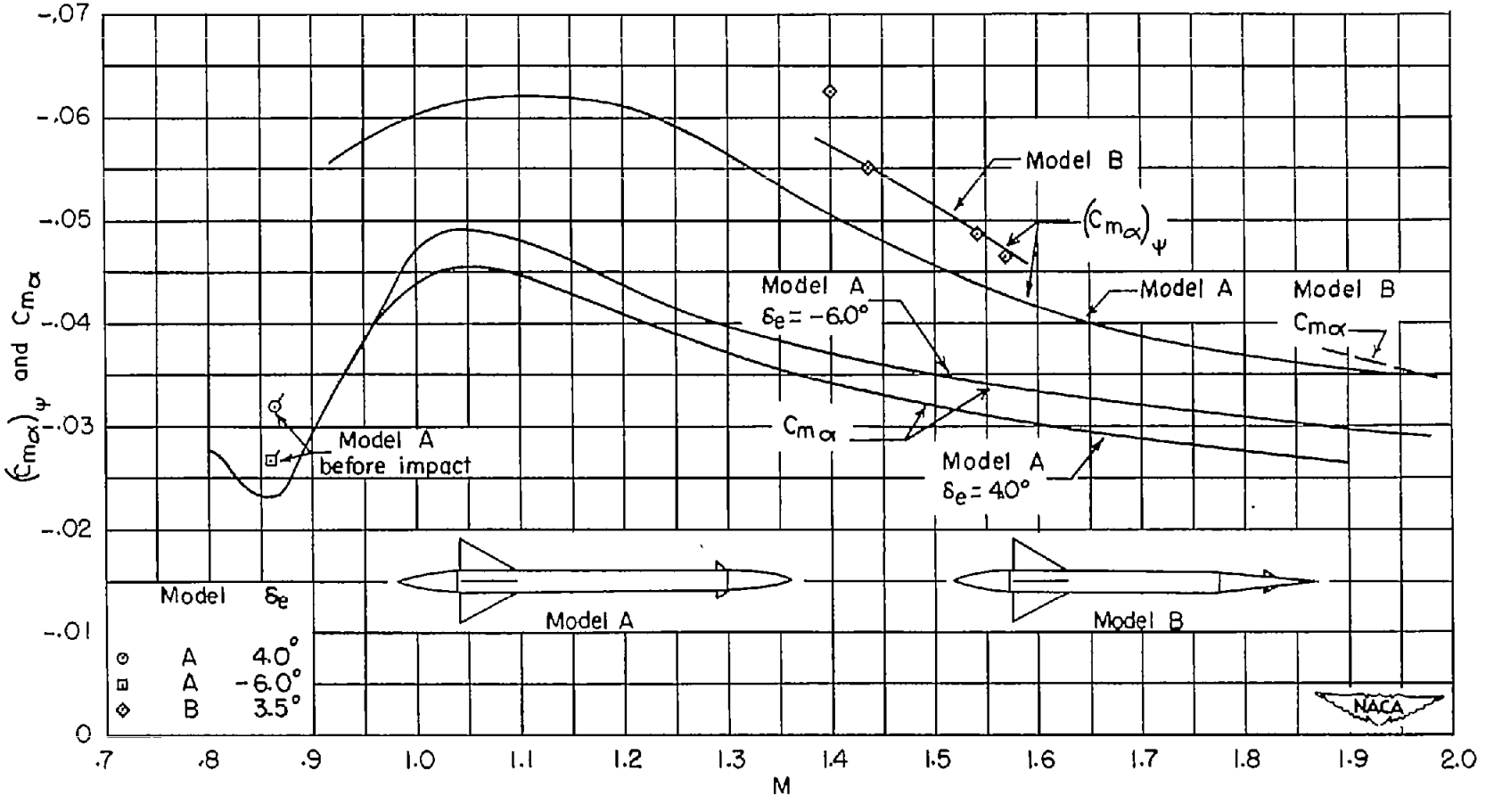

Figure 8.- Variation of static stability derivative C_{m_α} with Mach number.

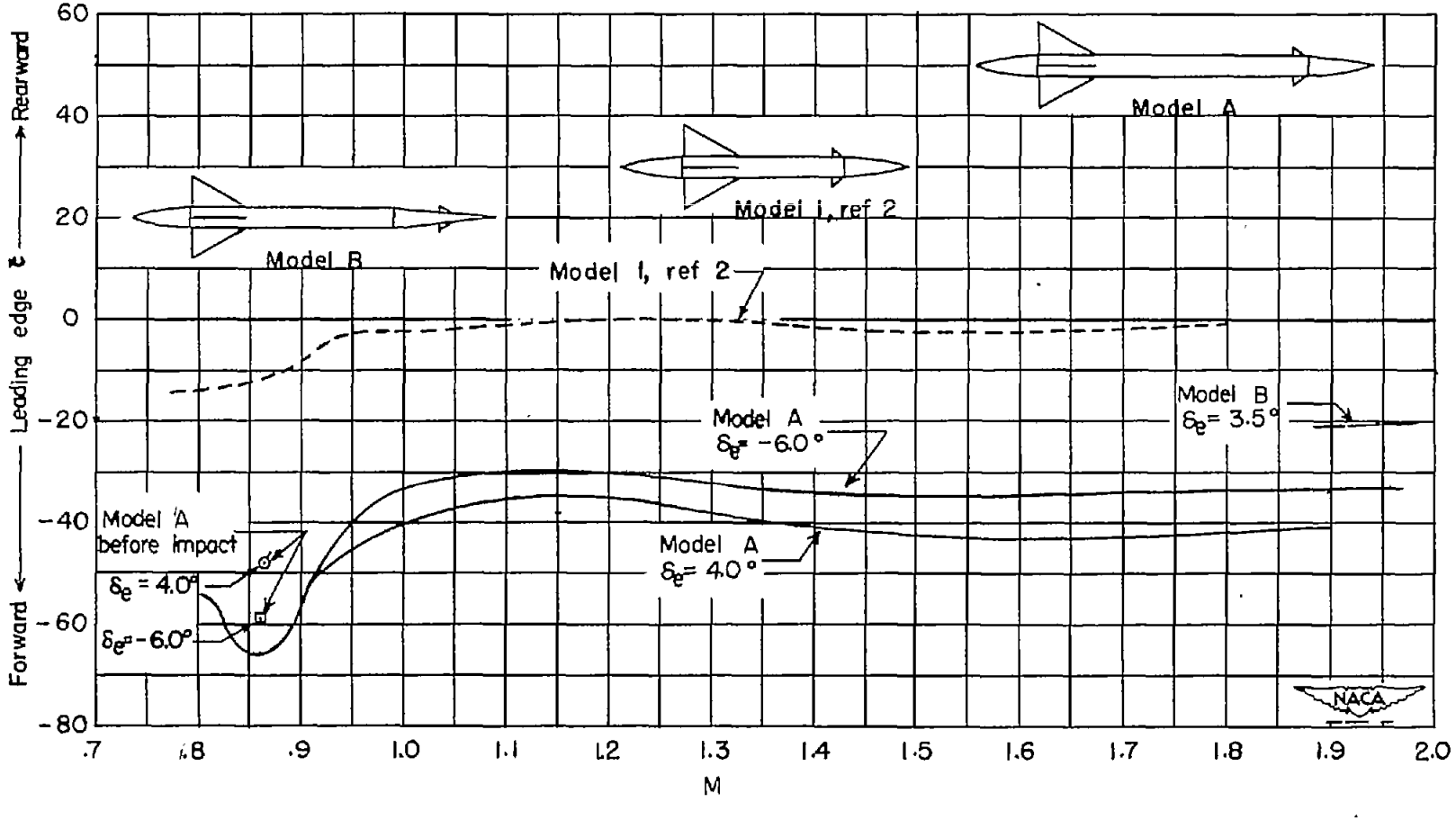

Figure 9.- Variation of aerodynamic center position with Mach number, percent of $\bar{c}$.

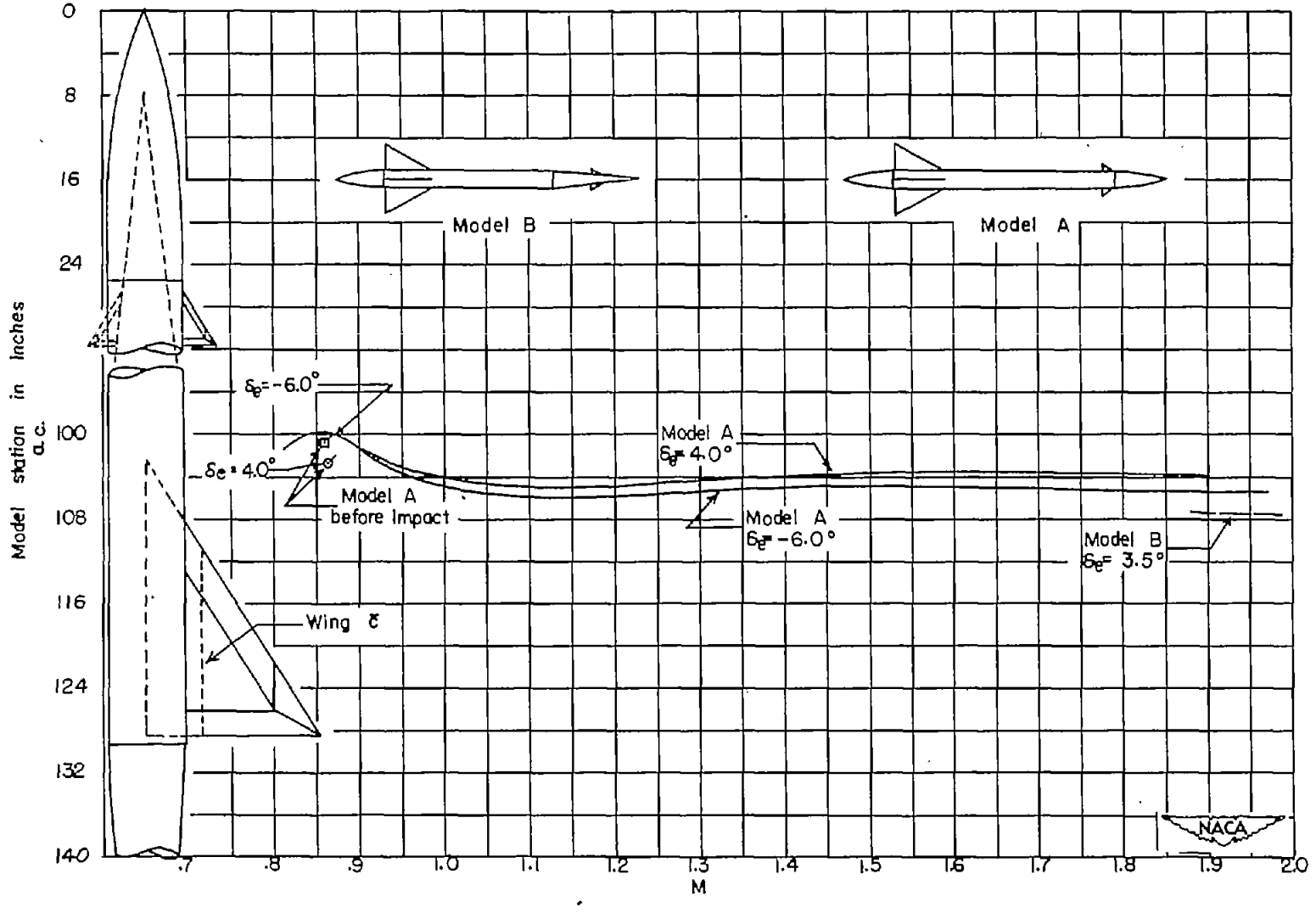

Figure 10.- Variation of aerodynamic center position with Mach number.

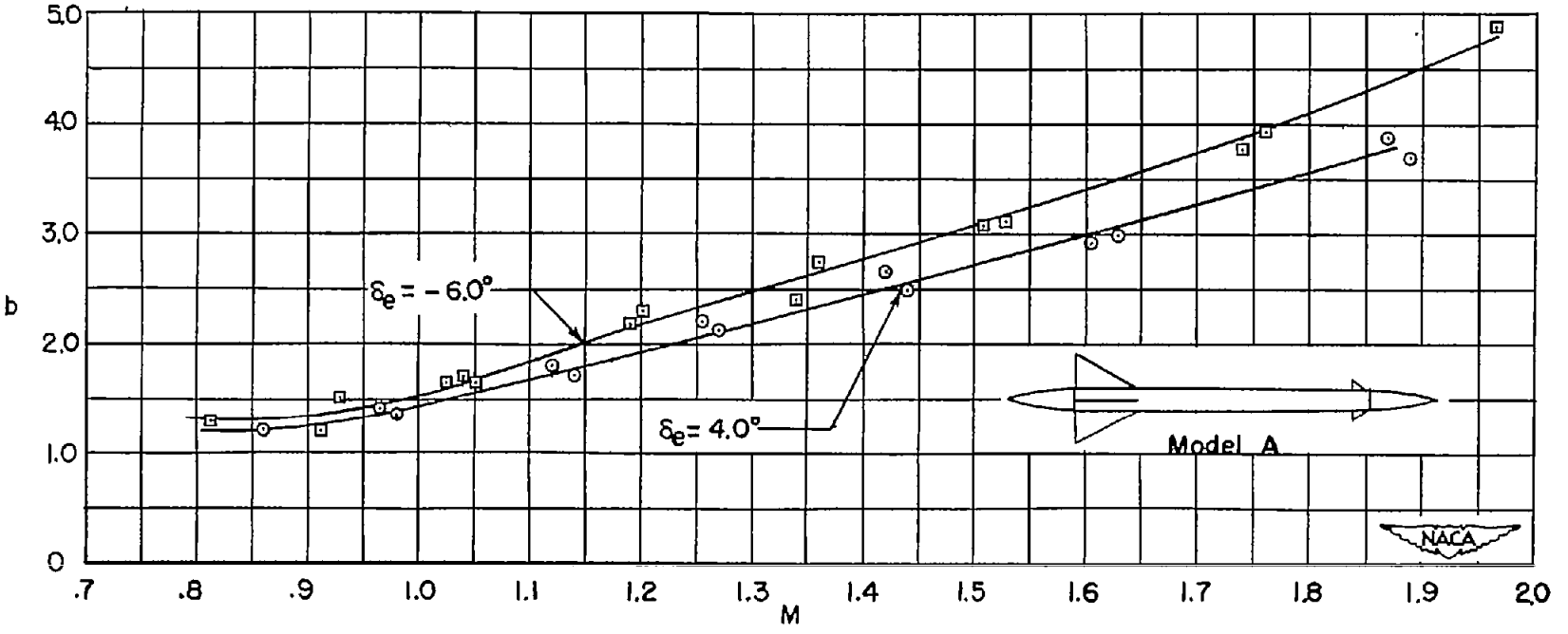

Figure 11.- Variation of exponential damping constant b with Mach number for model A.

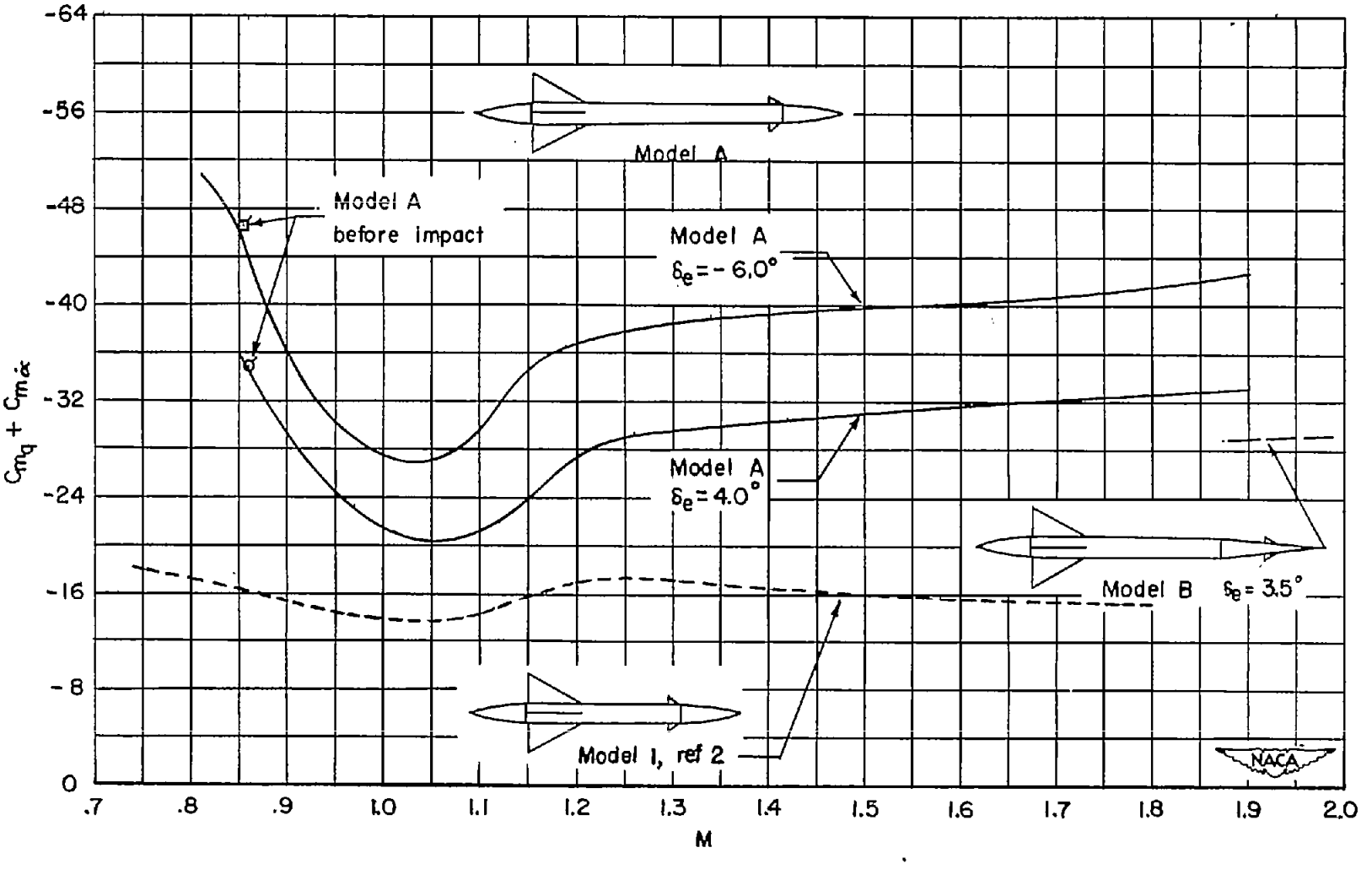

Figure 12.- Variation of aerodynamic damping-in-pitch derivative $C_{m_q} + C_{m_{\dot{\alpha}}}$ with Mach number.

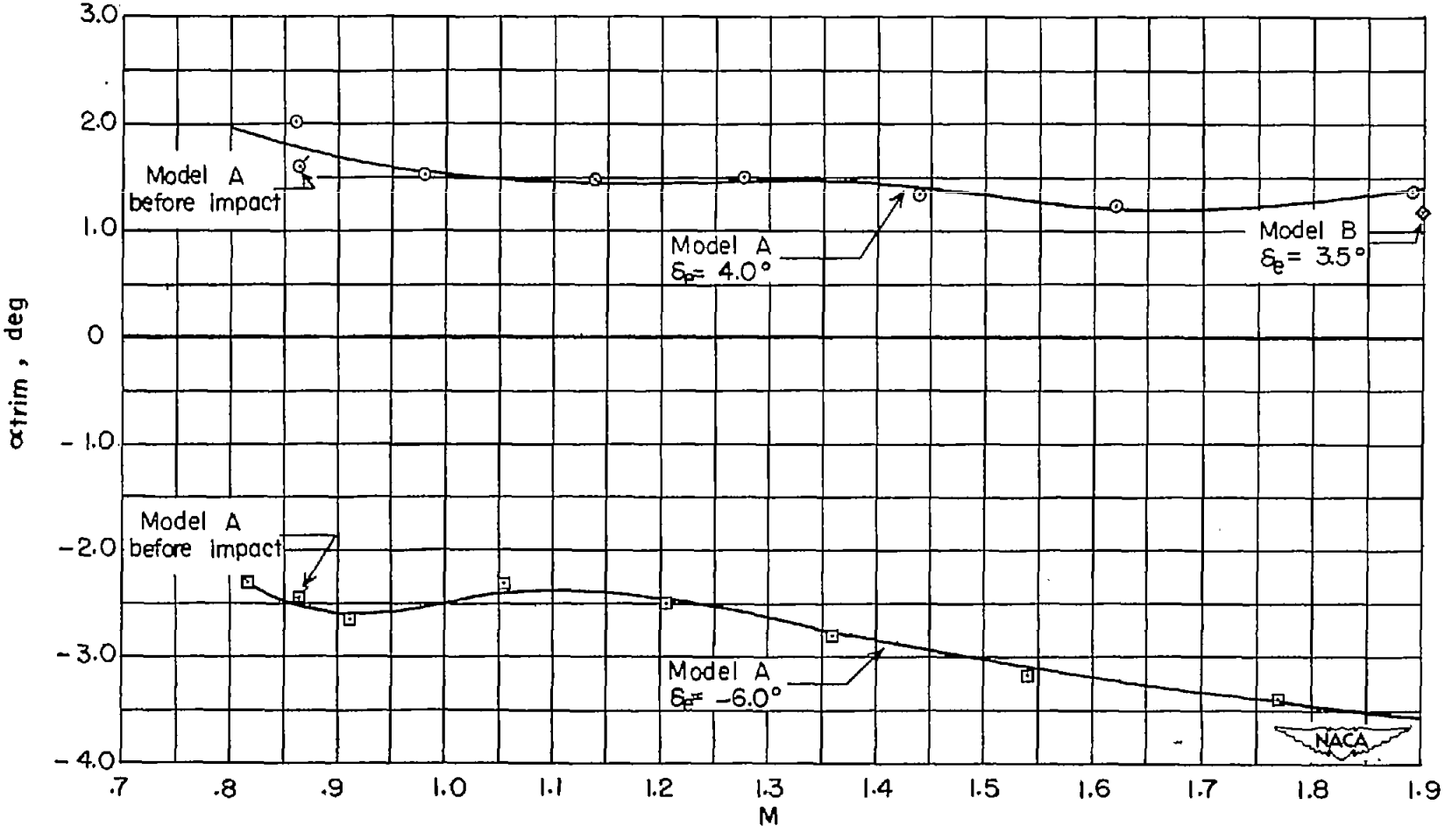

Figure 13.- Variation of trim angle of attack with Mach number.

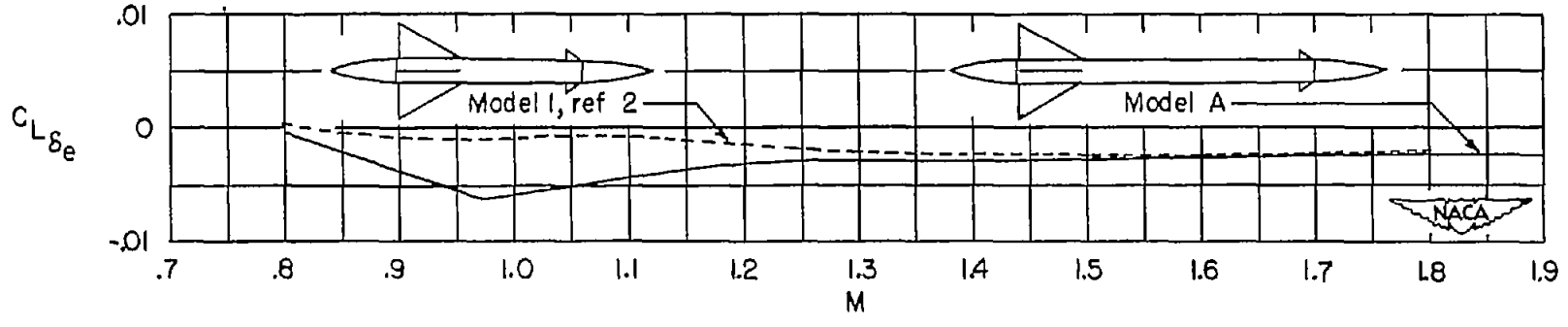

Figure 14.- Effectiveness of canard control surfaces in producing lift.

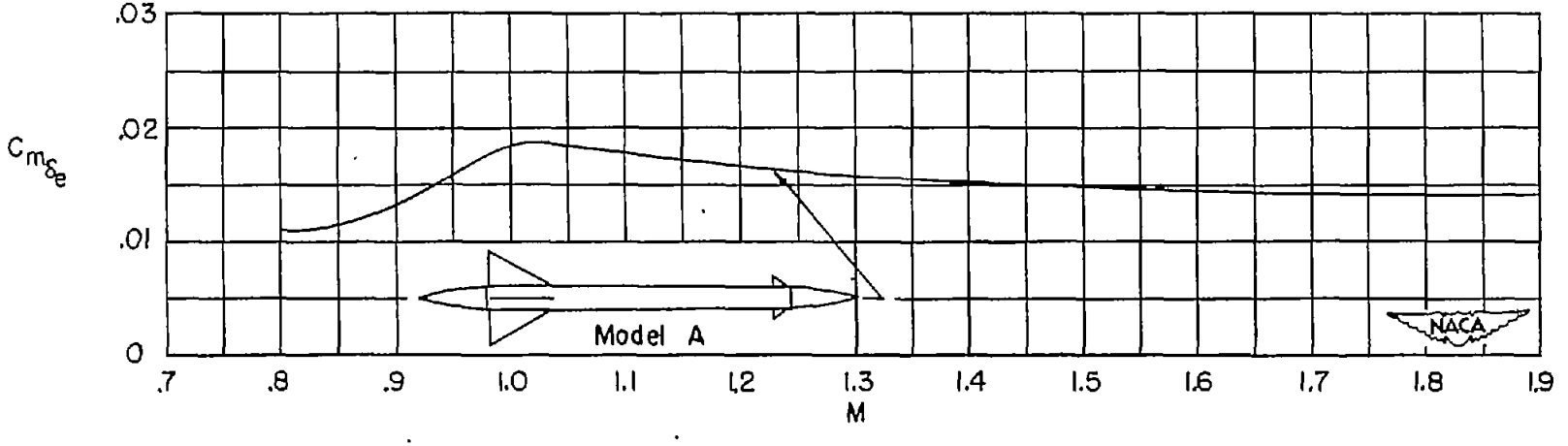

Figure 15.- Pitching effectiveness of canard control surfaces.

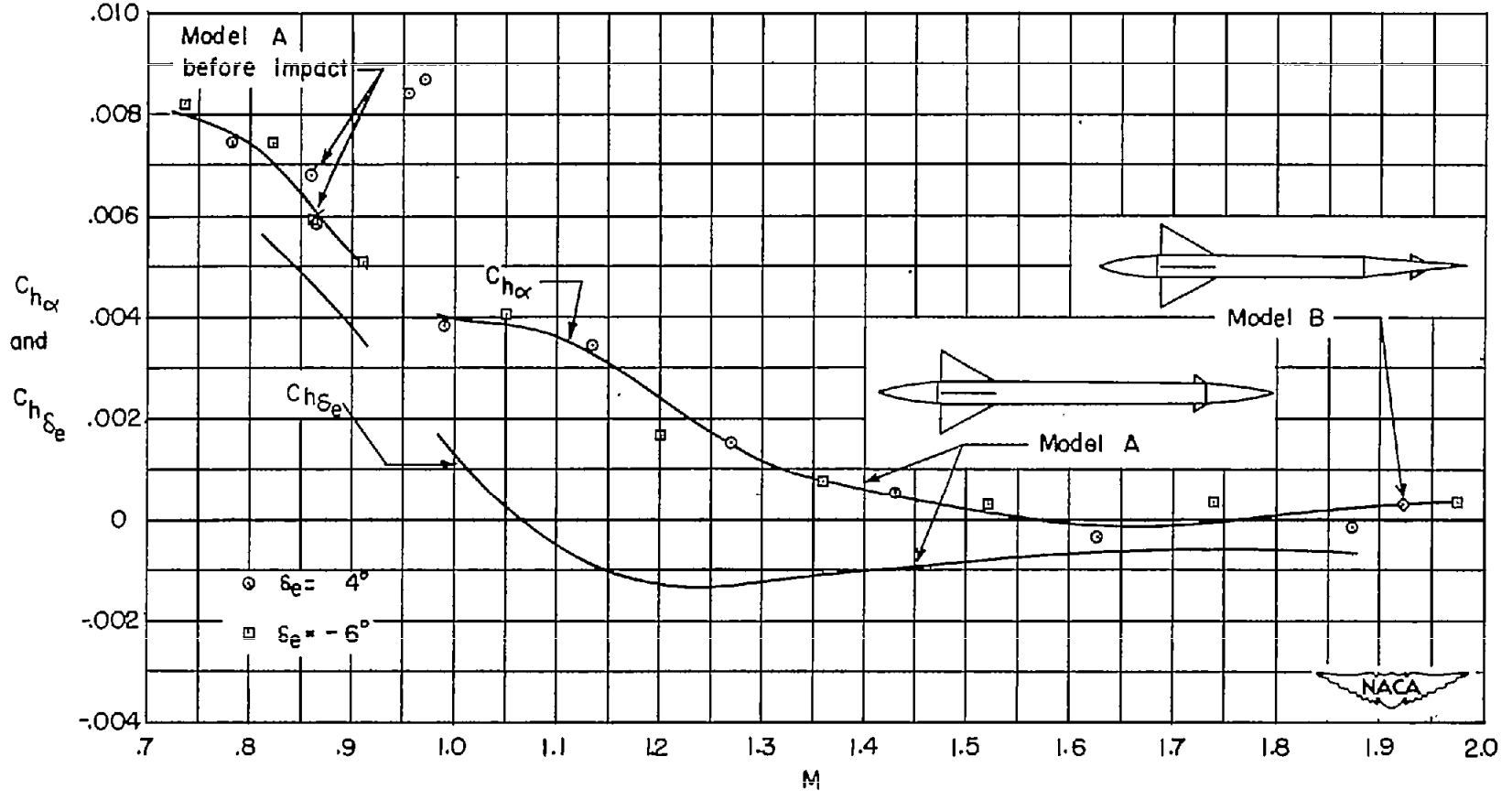

Figure 16.- Variation of hinge-moment coefficient derivatives C_{h_α} and C_{h_δ} with Mach number.

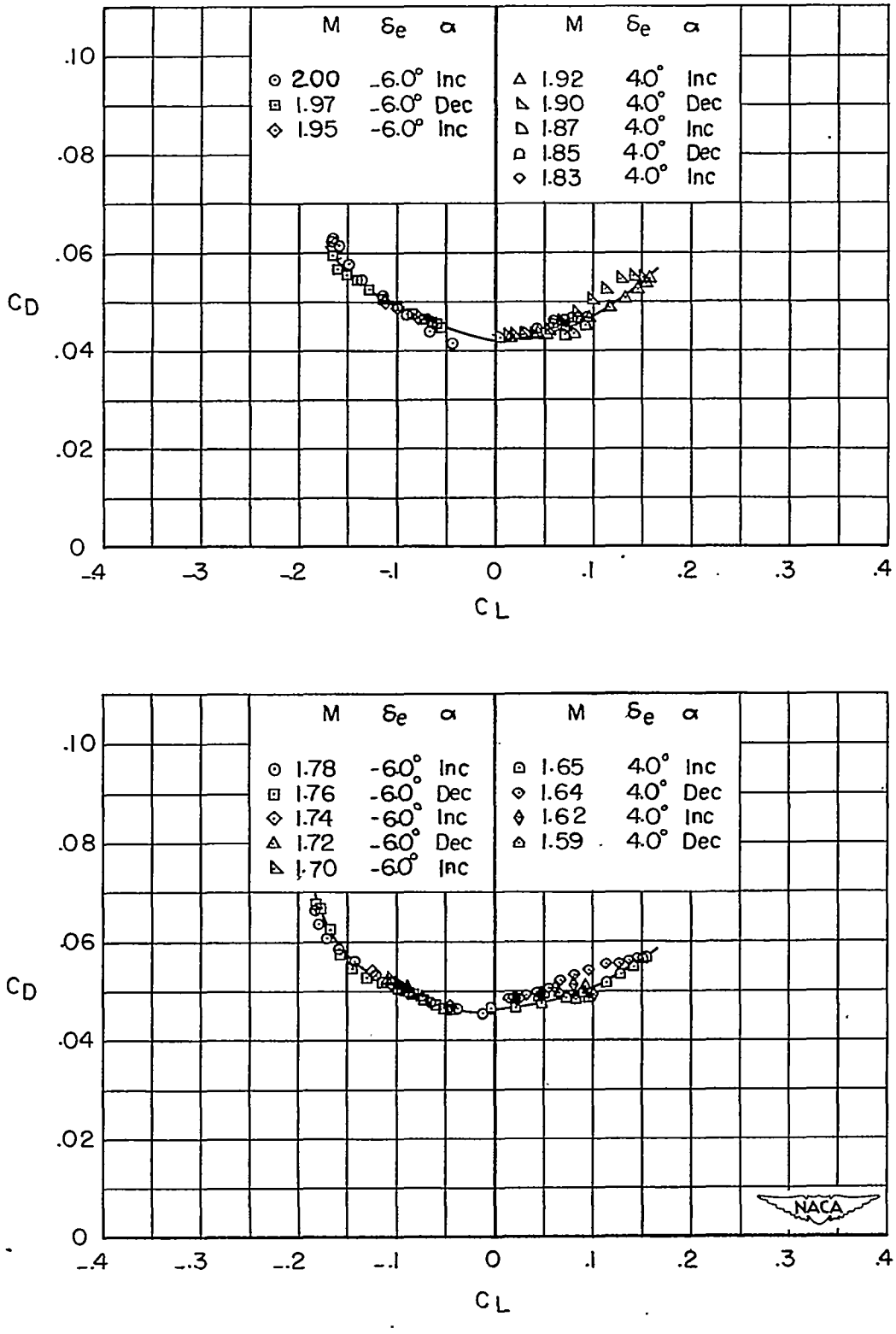

Figure 17.- Lift-drag polars for model A.

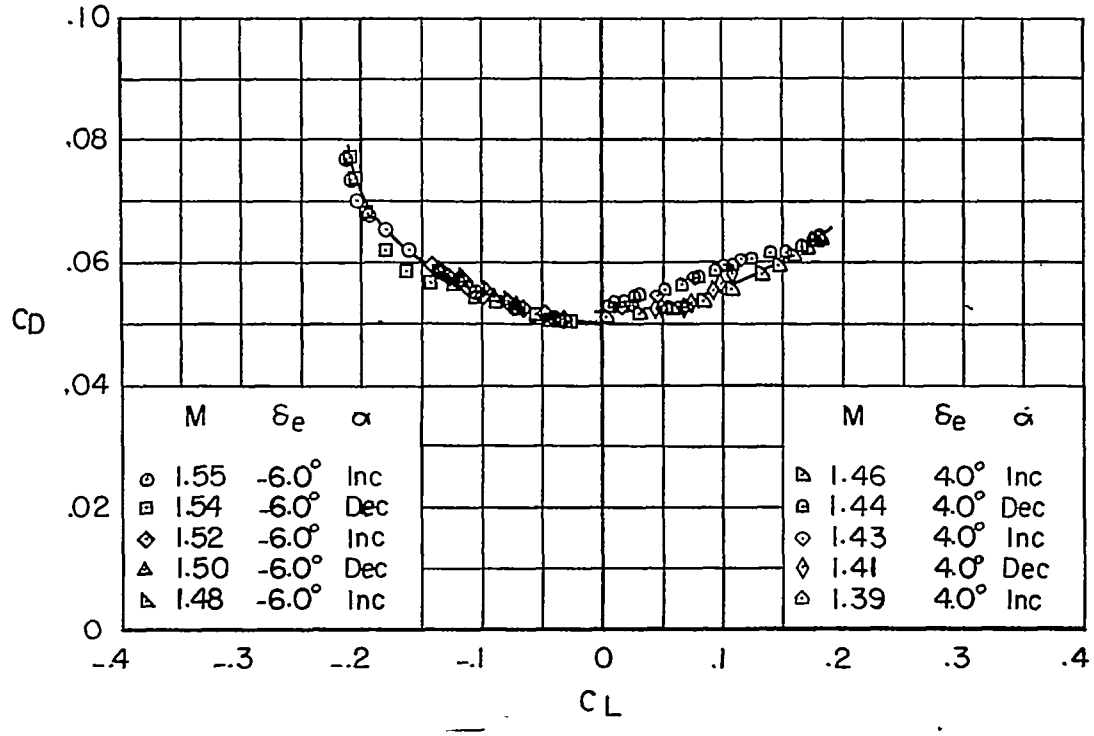

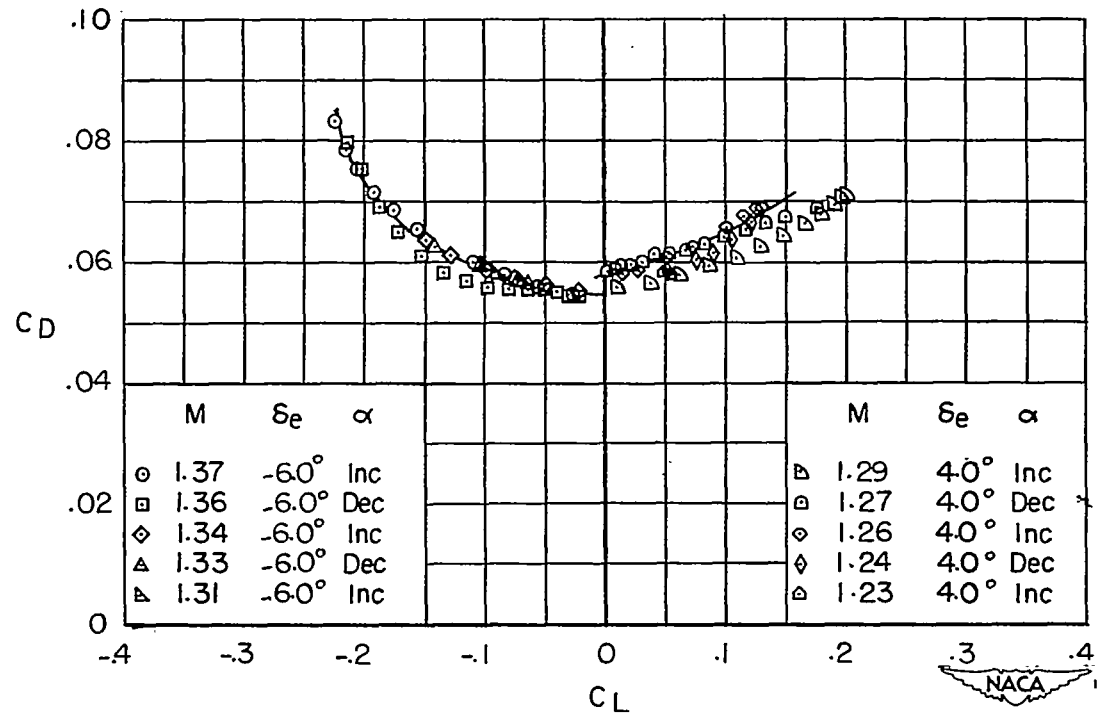

Figure 17.- Continued.

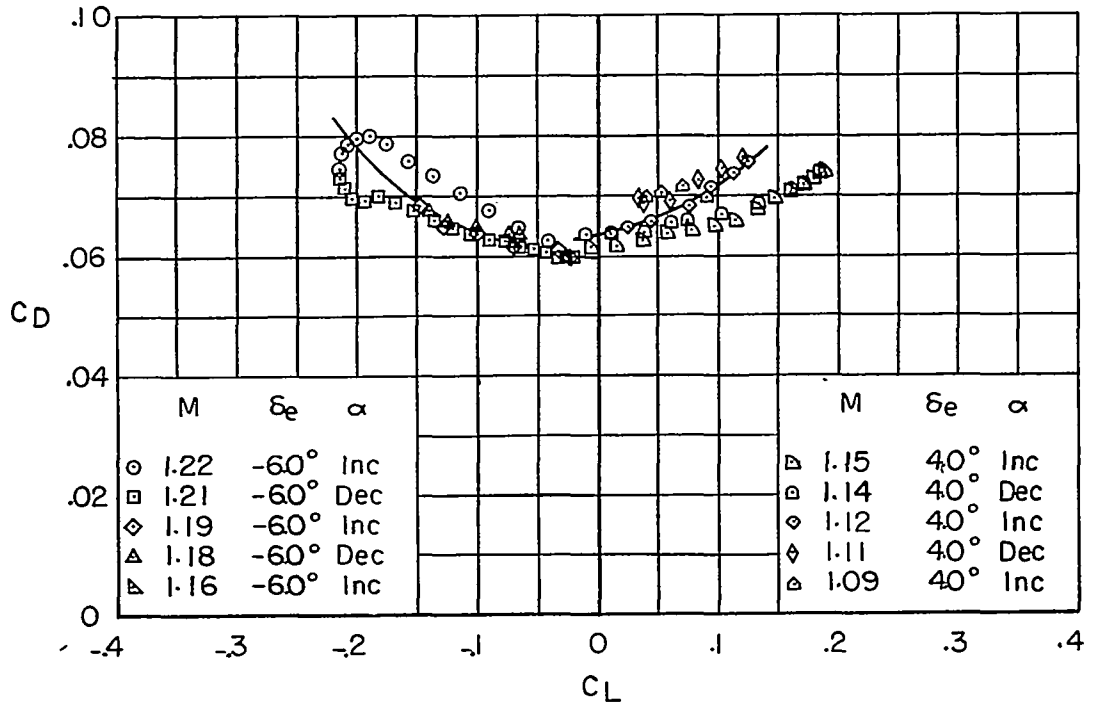

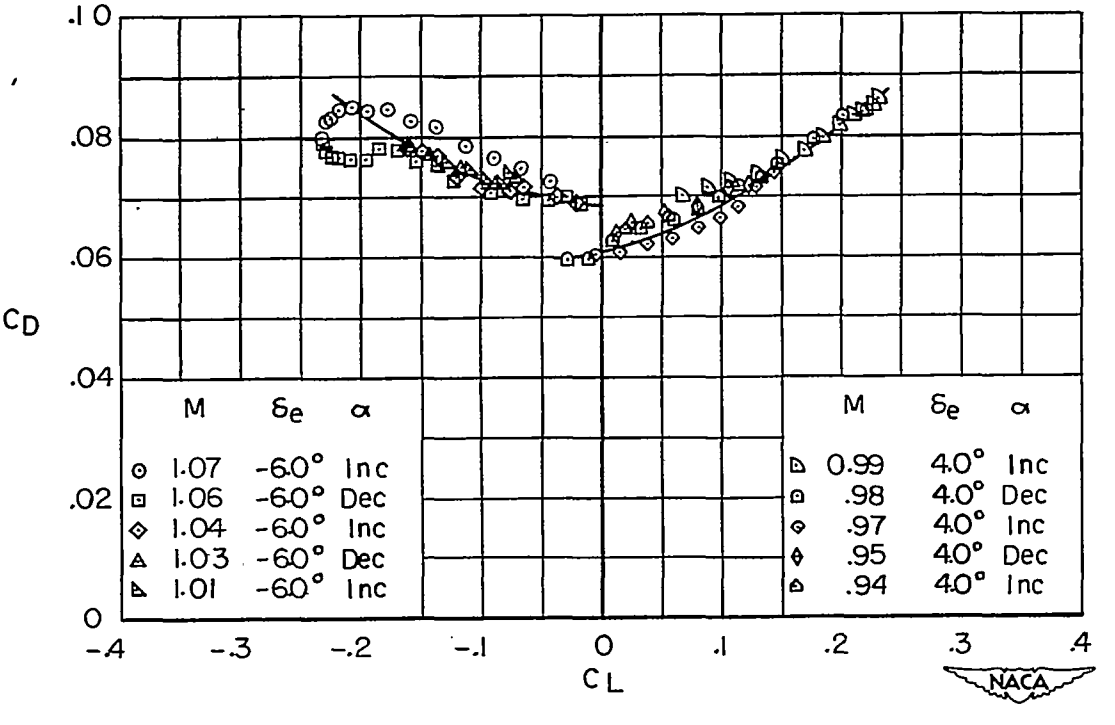

Figure 17.- Continued.

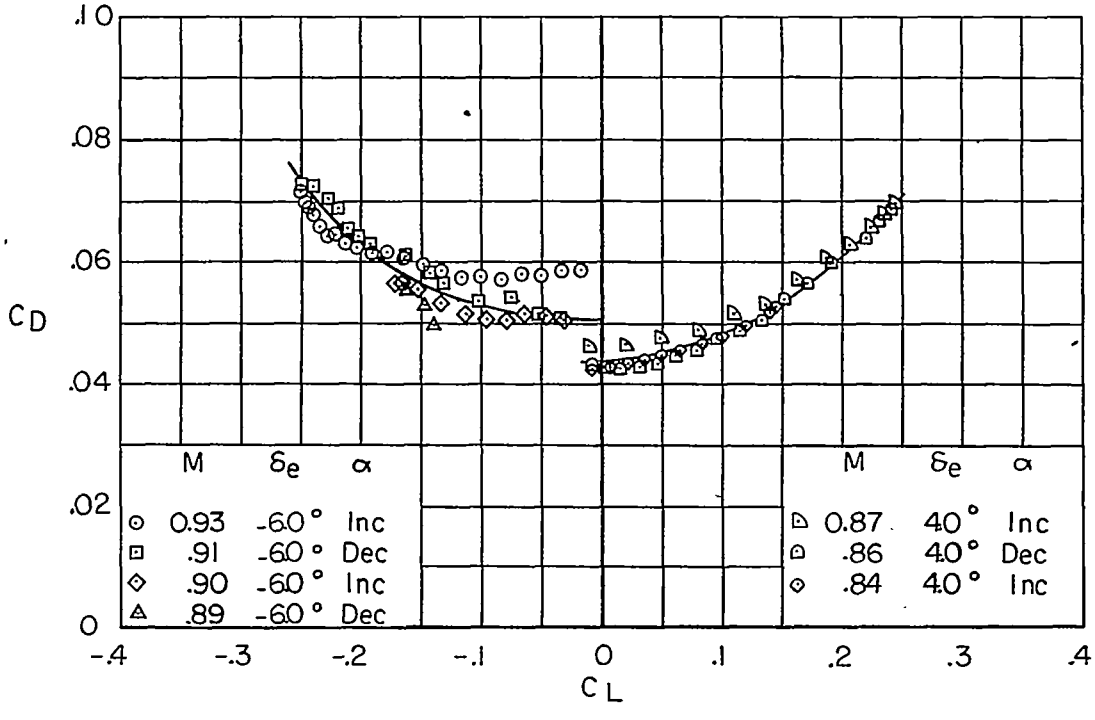

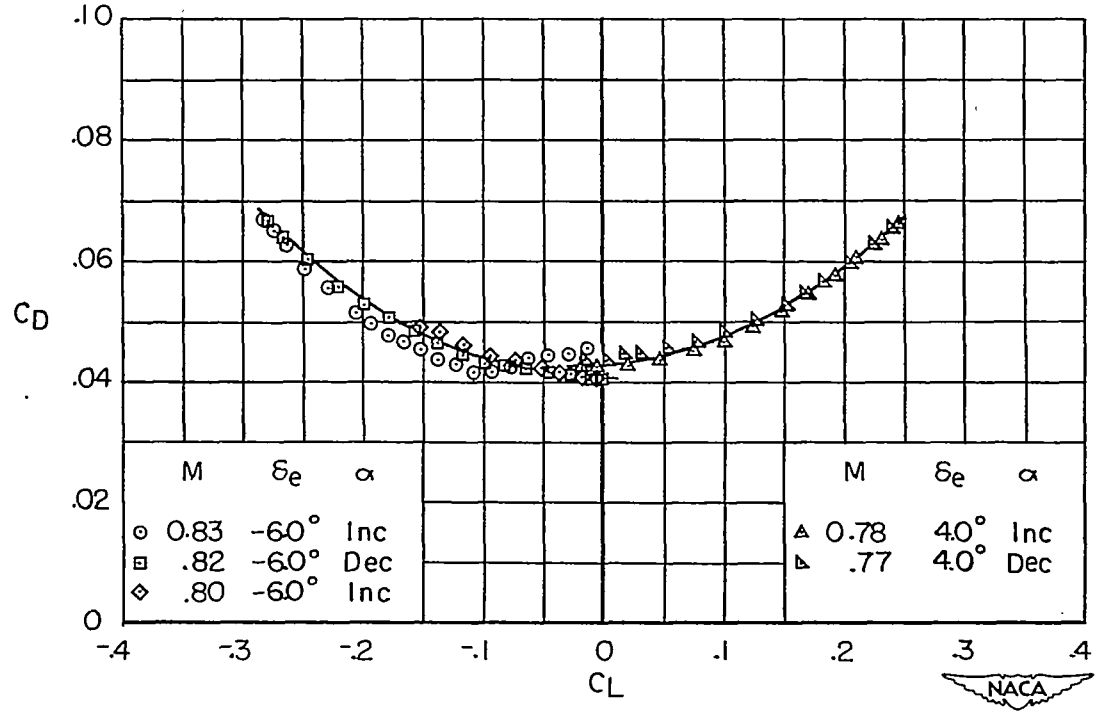

Figure 17.- Concluded.

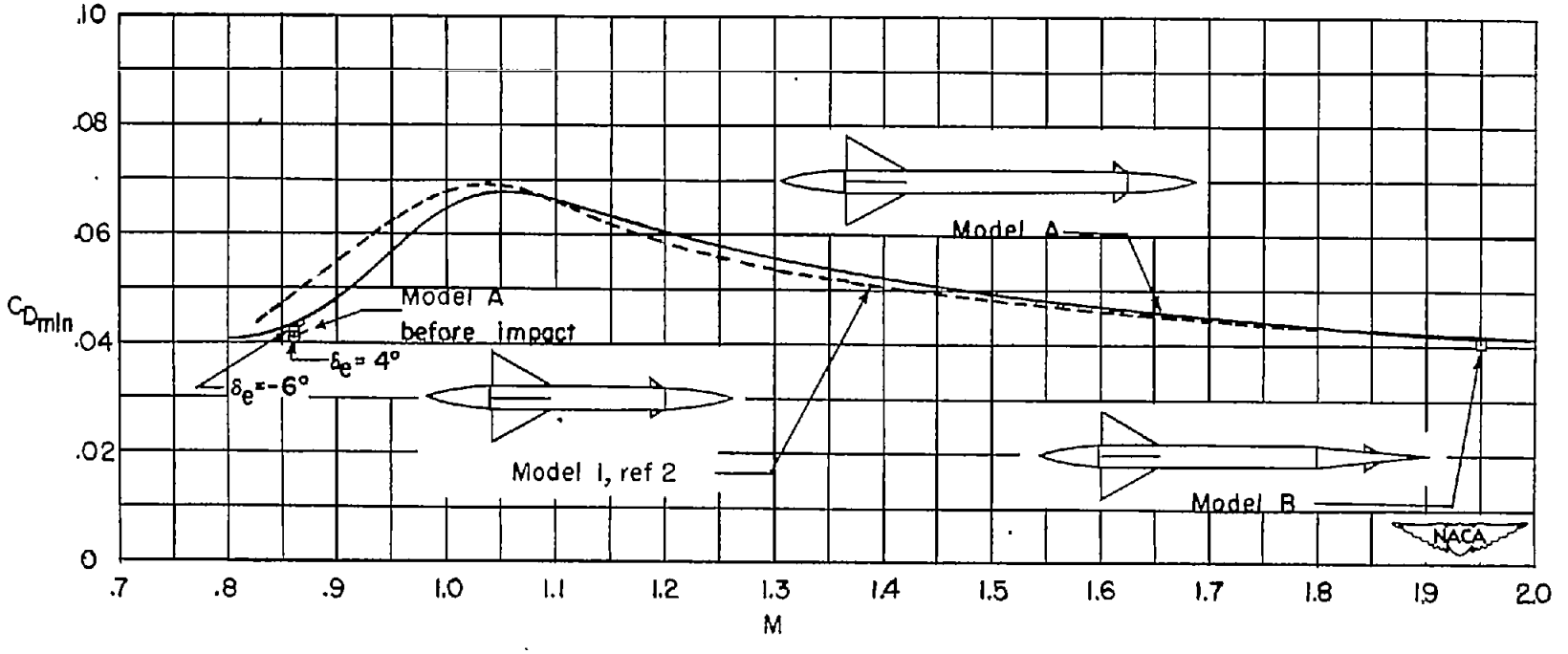

Figure 18.- Comparison of minimum drag coefficient of model tested with similar model having a shorter fuselage.

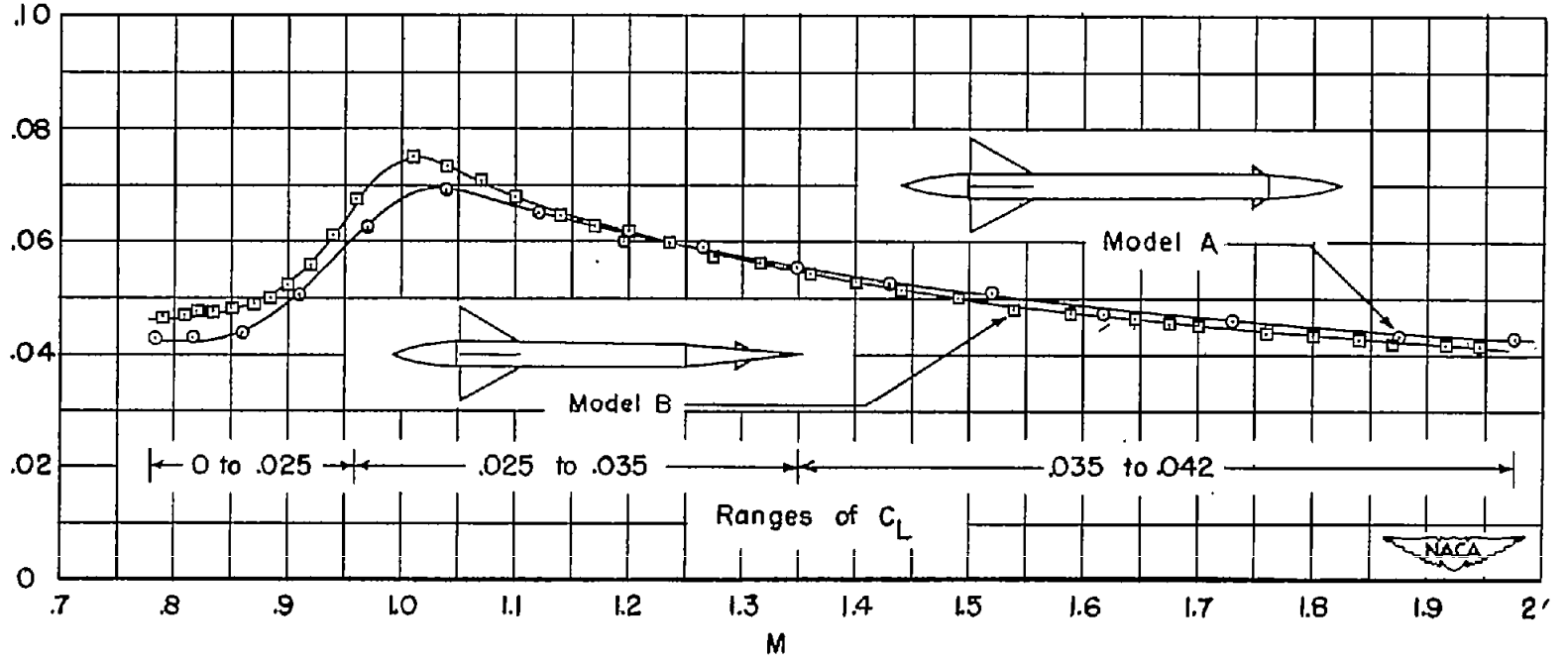

Figure 19.- Comparison of drag coefficient of models tested.

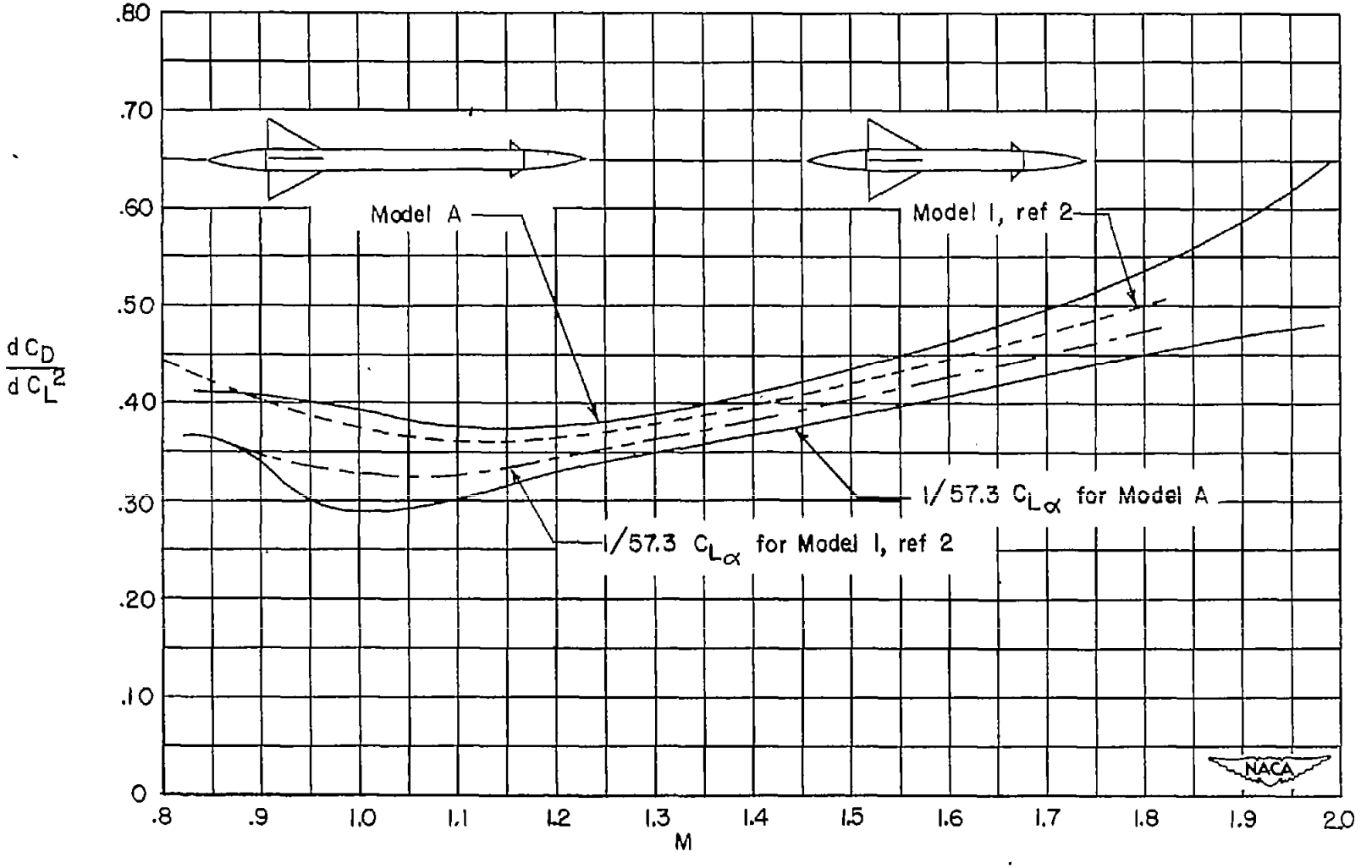

Figure 20.- Comparison of the effects of lift on drag of model tested with similar model having a shorter fuselage.

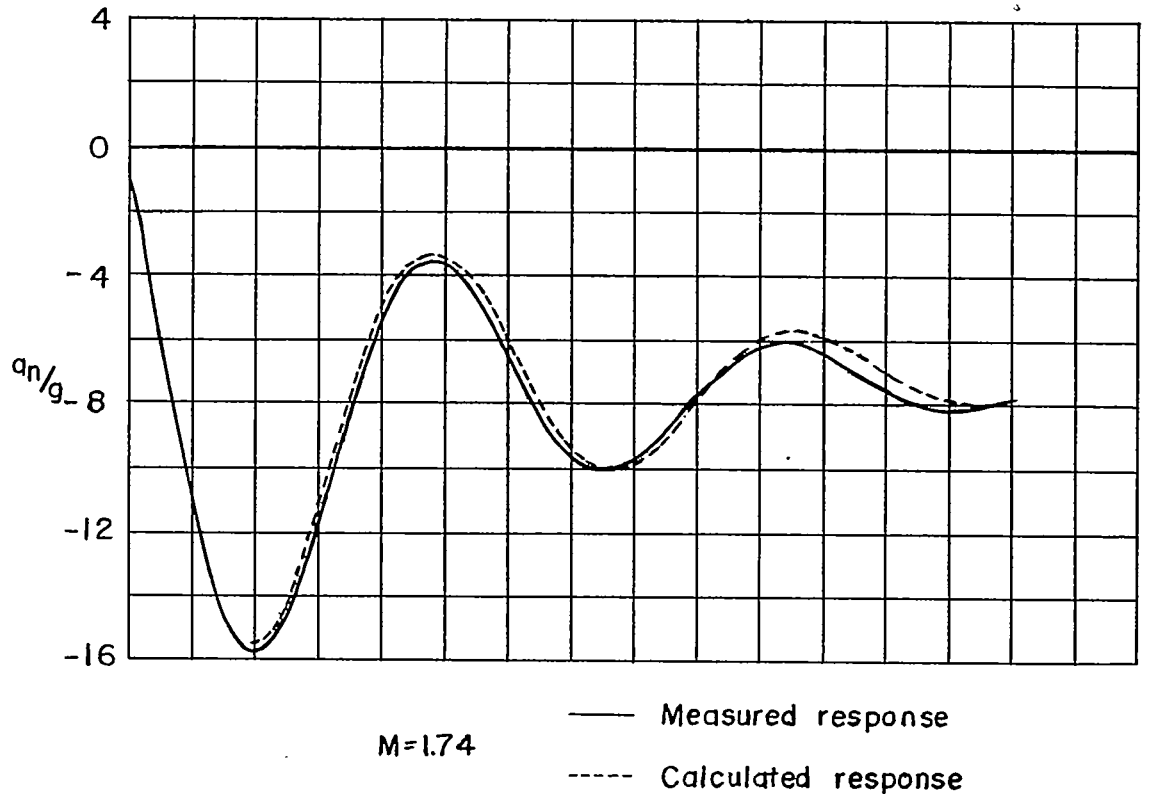

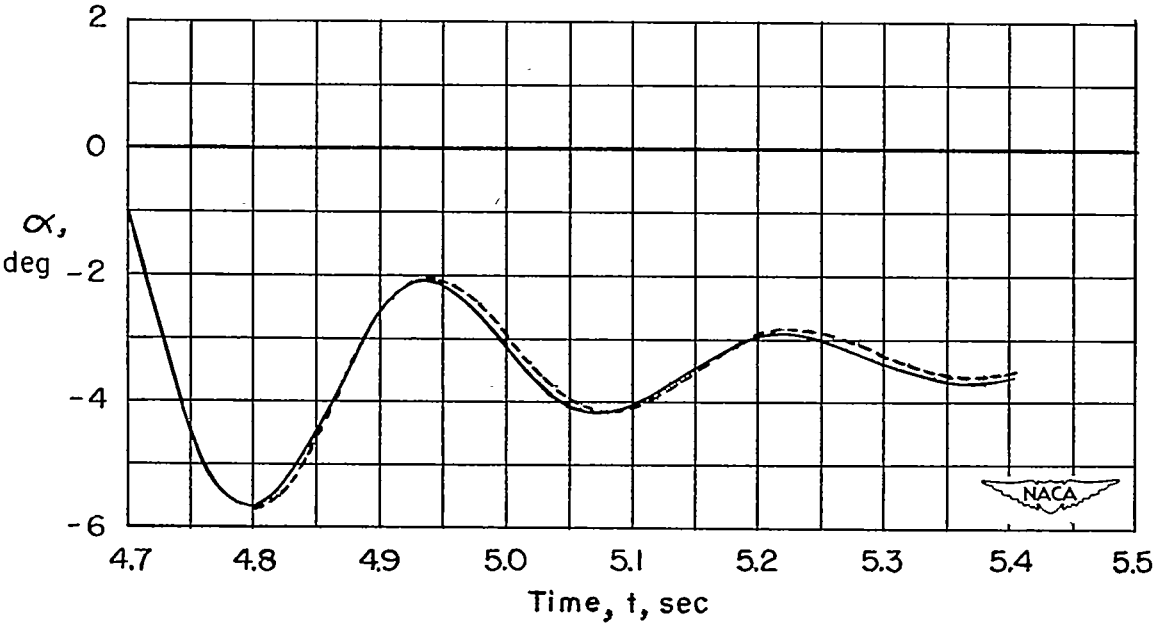

Figure 21.- Comparison of measured and calculated response curves. $\delta_e = -6^o$.

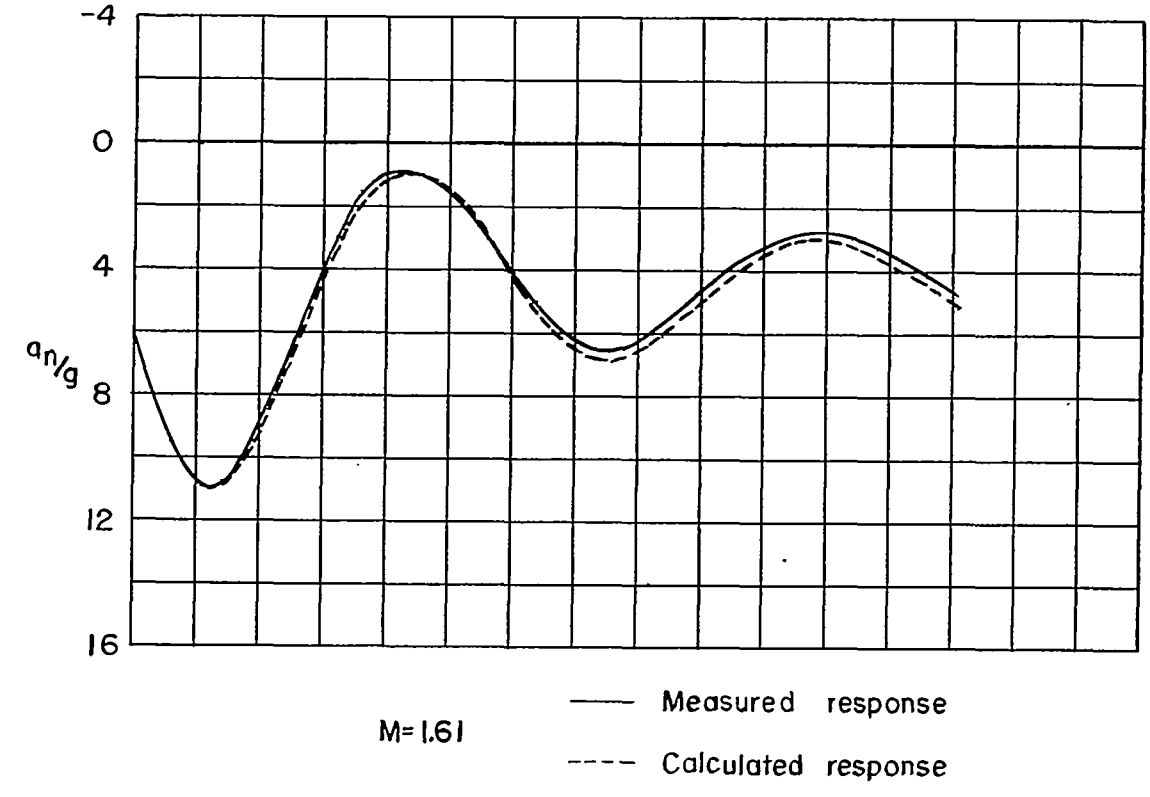

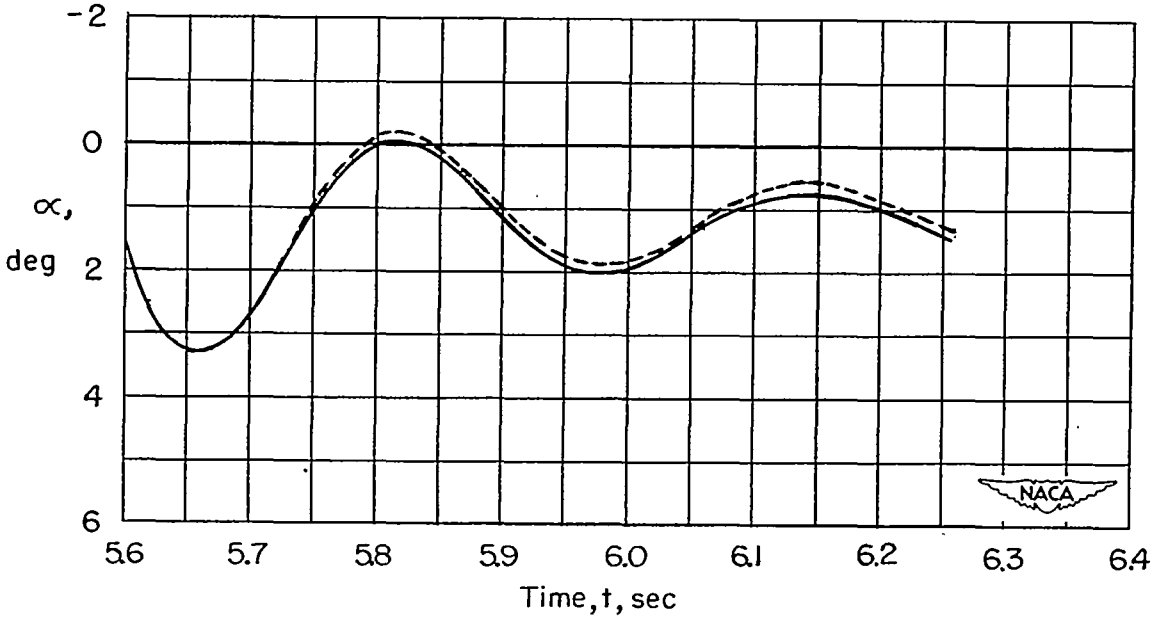

Figure 22.- Comparison of measured and calculated response curves. $\delta_e = 4^\circ$.

6K

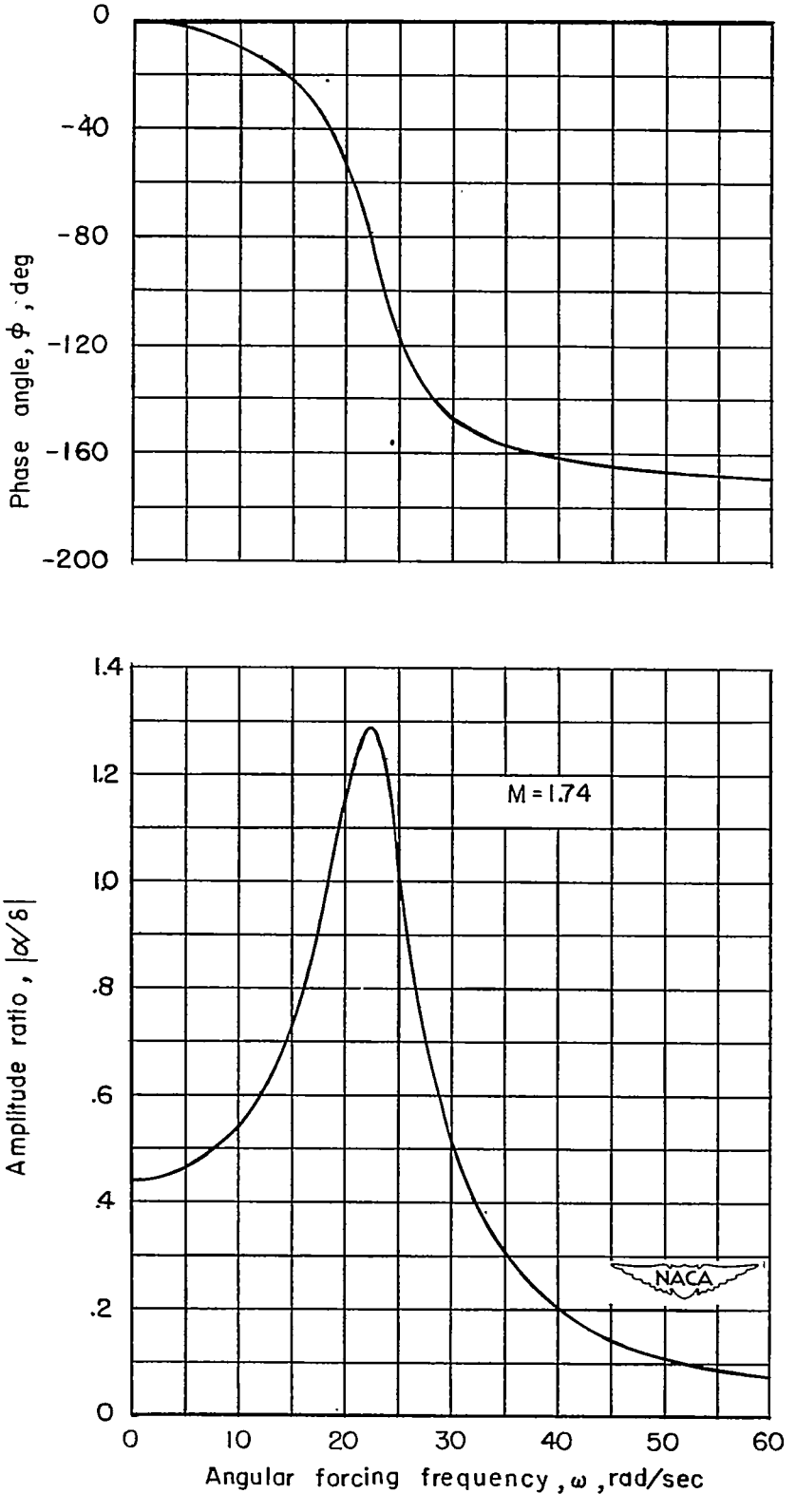

Figure 23.- Longitudinal frequency-response characteristics of model A for $\delta_e = -6^\circ$.

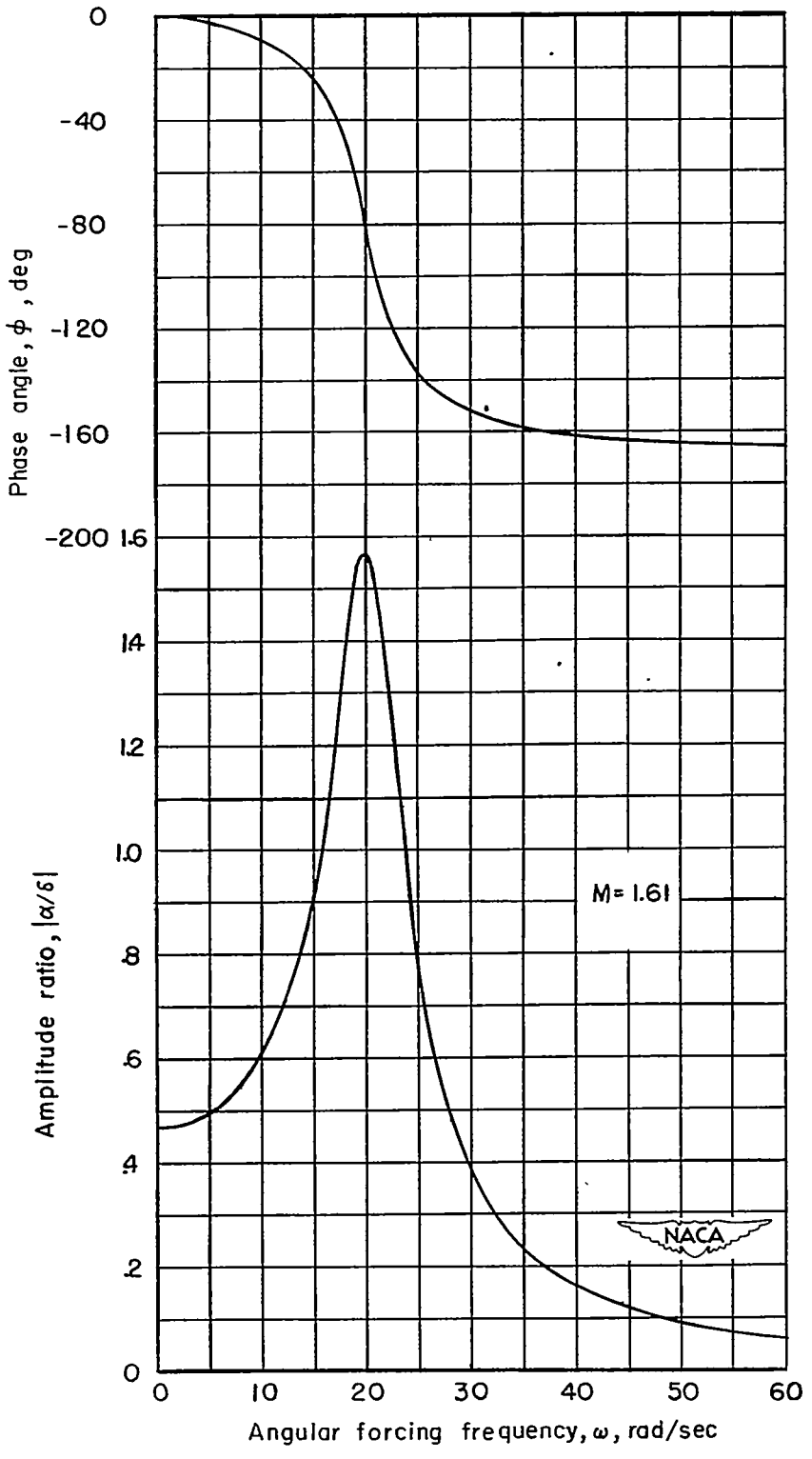

Figure 24.- Longitudinal frequency-response characteristics of model A for $\delta_e = 4^\circ$.

NACA-Langley - 6-20-52 - 350